Article

The extracellular matrix dictates regional competence for tumour initiation

https://doi.org/10.1038/s41586-023-06740-y

Received: 27 April 2022

Accepted: 11 October 2023

Published online: 15 November 2023

Check for updates

Nordin Bansaccal[1], Pauline Vieugue[1], Rahul Sarate[1], Yura Song[1], Esmeralda Minguijon[2], Yekaterina A. Miroshnikova[3,4], Dagmar Zeuschner[4], Amandine Collin[5], Justine Allard[5], Dan Engelman[1], Anne-Lise Delaunois[1], Mélanie Liagre[1], Leona de Groote[1], Evy Timmerman[6], Delphi Van Haver[6], Francis Impens[6], Isabelle Salmon[2,5], Sara A. Wickström[4,7], Alejandro Sifrim[8] & Cédric Blanpain[1,9]✉

The skin epidermis is constantly renewed throughout life[1,2]. Disruption of the balance between renewal and differentiation can lead to uncontrolled growth and tumour initiation[3]. However, the ways in which oncogenic mutations affect the balance between renewal and differentiation and lead to clonal expansion, cell competition, tissue colonization and tumour development are unknown. Here, through multidisciplinary approaches that combine in vivo clonal analysis using intravital microscopy, single-cell analysis and functional analysis, we show how SmoM2—a constitutively active oncogenic mutant version of Smoothened (SMO) that induces the development of basal cell carcinoma—affects clonal competition and tumour initiation in real time. We found that expressing SmoM2 in the ear epidermis of mice induced clonal expansion together with tumour initiation and invasion. By contrast, expressing SmoM2 in the back-skin epidermis led to a clonal expansion that induced lateral cell competition without dermal invasion and tumour formation. Single-cell analysis showed that oncogene expression was associated with a cellular reprogramming of adult interfollicular cells into an embryonic hair follicle progenitor (EHFP) state in the ear but not in the back skin. Comparisons between the ear and the back skin revealed that the dermis has a very different composition in these two skin types, with increased stiffness and a denser collagen I network in the back skin. Decreasing the expression of collagen I in the back skin through treatment with collagenase, chronic UV exposure or natural ageing overcame the natural resistance of back-skin basal cells to undergoing EHFP reprogramming and tumour initiation after SmoM2 expression. Altogether, our study shows that the composition of the extracellular matrix regulates how susceptible different regions of the body are to tumour initiation and invasion.

The skin epidermis is an essential barrier that protects animals against the external environment. The interfollicular epidermis (IFE) is a stratified epithelium that contains a proliferative basal layer and several differentiated suprabasal layers[1,2]. During homeostasis, the loss of differentiated cells on the skin surface is compensated by proliferation to maintain a constant number of cells[3]. The generation of new cells is ensured by stem cells and progenitors that divide asymmetrically at the population level[3]. Previous lineage-tracing and clonal-analysis studies have revealed that the balance between renewal and differentiation is achieved by the relative proportions of asymmetric renewal, symmetric renewal and symmetric differentiation in stem cells and progenitor cells[3]. During homeostasis, symmetric renewal and symmetric differentiation are perfectly balanced. The deregulation of this exquisite balance between proliferation and differentiation can have disastrous outcomes, such as cancer initiation[3].

Basal cell carcinoma (BCC) is the most frequently occurring form of human cancer, with more than five million new cases diagnosed each year worldwide[4]. BCCs arise from the activation of the Hedgehog pathway by either loss-of-function mutations in the Patched 1 (*PTCH1*) gene or gain-of-function mutations in the Smoothened (*SMO*) gene[4]. Mouse models of BCC using *Ptch1* deletion or the expression of oncogenic mutant *Smo* (SmoM2) lead to the formation of tumours that resemble superficial human BCC[5]. Expressing SmoM2 in the skin epidermis leads to the development of BCC in the tail and ear epidermis[6,7].

Cell competition is a biological process that leads to the elimination of one population of loser cells by a population of winner cells[8–10]. It has

[1]Laboratory of Stem Cells and Cancer, Université Libre de Bruxelles, Brussels, Belgium. [2]Department of Pathology, CUB Hôpital Erasme, Hôpital Universitaire de Bruxelles, Université Libre de Bruxelles (ULB), Brussels, Belgium. [3]Laboratory of Molecular Biology, National Institute of Diabetes and Digestive and Kidney Diseases, National Institutes of Health, Bethesda, MD, USA. [4]Max Planck Institute for Molecular Biomedicine, Münster, Germany. [5]DIAPath, Center for Microscopy and Molecular Imaging (CMMI), Université Libre de Bruxelles (ULB), Gosselies, Belgium. [6]VIB Center for Medical Biotechnology, VIB Proteomics Core, Department of Biomolecular Medicine, Ghent University, Ghent, Belgium. [7]Stem Cells and Metabolism Research Program, Faculty of Medicine, University of Helsinki, Helsinki, Finland. [8]Department of Human Genetics, KU Leuven, Leuven, Belgium. [9]WELBIO, Université Libre de Bruxelles (ULB), Brussels, Belgium. ✉e-mail: Cedric.Blanpain@ulb.be

been proposed that oncogene-expressing cells can outcompete their wild-type neighbours to allow tumour formation, similar to what has been described as super-competition in fly imaginal discs expressing different levels of dMyc (refs. 11,12). However, the exact mechanisms by which oncogene-expressing cells induce cell competition with their wild-type neighbours and allow tumour initiation remain poorly understood. Sequencing studies have shown that oncogenic mutations occur at a notably high frequency in tissues that appear histologically normal[13]. The existence of oncogenic mutations in histologically normal tissues suggests that mutations alone are not sufficient to drive neoplastic growth, and that other unknown mechanisms promote or restrain the progression of oncogene-expressing cells into malignant invasive tumours. The question of whether all oncogene-targeted clones present the same ability to outcompete their wild-type neighbours remains poorly understood.

Here, using multidisciplinary approaches that combine lineage tracing, clonal analysis in living animals, single-cell sequencing, quantitative proteomics and functional experiments, we investigate the mode of cell competition and the ability of oncogene-expressing cells to develop invasive BCC in different skin regions.

Intravital imaging of SmoM2 clones

It has been reported that the expression of SmoM2 in the back skin does not lead to BCC formation[6,7], but why the back-skin epidermis is not competent for BCC initiation is unknown. One hypothesis is that stem cells in the back skin do not undergo symmetric division and clonal expansion after the expression of oncogenic SmoM2, leading to their inability to outcompete their wild-type neighbours. To investigate the effect of the oncogenic mutation on cell competition, clonal expansion and competence to induce tumour initiation in different locations of the body, we sought to develop a mouse model that would enable us to monitor the fate of single oncogene-targeted clones over time in living mice, using intravital multiphoton confocal microscopy. To this end, we generated a mouse model that allows the expression of the SmoM2 oncogene together with a fluorescent reporter gene that can be monitored by intravital microscopy. In the absence of oncogene expression, all epidermal cells express the tdTomato fluorescent protein at the membrane in K14Cre^{ER}/Rosa-SmoM2-YFP/Rosa-mT/mG mice. After administration of tamoxifen, CreER-mediated recombination induces the expression of SmoM2 and a switch of the reporter gene from the red fluorescent to a green fluorescent protein (GFP) (Fig. 1a–f). To track the same cells over time, we used a tattoo to identify the precise skin regions and defined the cell coordinates using the stable pattern of hair-follicle arrangement found in the epidermis, which allowed us to monitor the same clones in anaesthetized mice (Extended Data Fig. 1a–e).

We monitored the fate of SmoM2-expressing cells over time in the ear, a skin location associated with BCC formation. Compared to wild-type cells, which divide asymmetrically at the population level[14–16], SmoM2 expression promoted self-renewing division, leading to an increasing pool of basal cells that first expand laterally, together with a block in suprabasal differentiation[14]. About three weeks after the expression of SmoM2, the shape of the oncogene-expressing cells changed, and the clones adopted a placode-like morphology, which grew progressively downwards and invaded the dermis (Fig. 1a,b). After six weeks, SmoM2-expressing clones continued their vertical expansion and invaded the dermis in a branch-like structure, reminiscent of the growth of superficial BCC found in the mouse tail epidermis and in human skin[5,6] (Fig. 1c). Consistent with this invasive phenotype and a previous study[17], immunostaining components of the basal lamina (α6 integrin and laminin 332) and electron microscopy analysis showed that there is a discontinuity of the basal lamina at the leading edge of invading SmoM2 clones in the ear (Extended Data Fig. 2a–e). Quantification of the lateral size, depth of invasion and number of cells per clone showed that after the initial phase of lateral spreading (three weeks), SmoM2 clones minimally expanded laterally and continued to grow vertically by invading the dermis (Fig. 1g–i and Extended Data Fig. 2f–i). To further substantiate that SmoM2 expression increases self-renewing division, we performed short-term lineage tracing using BrdU pulse chase and

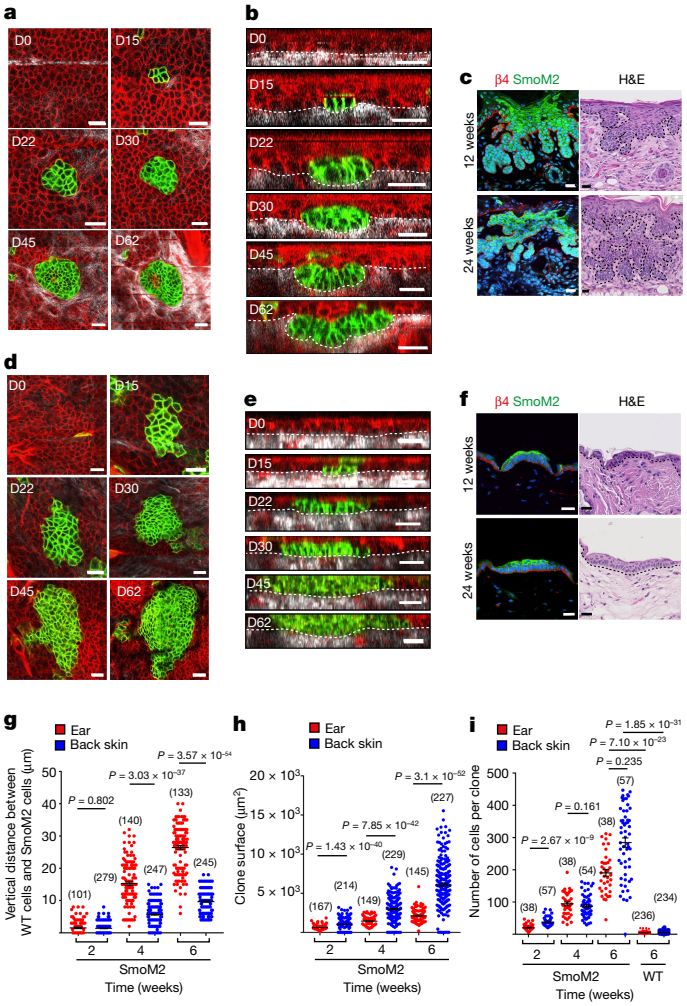

Fig. 1 | Intravital imaging of clonal expansion and BCC formation in the ear and in the back skin. a,**d**, Intravital imaging of the same SmoM2-expressing clone in the ear (**a**) and back skin (**d**) at different time points after tamoxifen administration to K14Cre^{ER}/Rosa-SmoM2-YFP/Rosa-mT/mG mice. Red, wild-type (WT) cells; green, SmoM2 cells; grey, second harmonic generation (SHG) signal. **b**,**e**, Orthogonal views of the same clone as in Fig. 1a,d, showing the invasion of the mutated clones over time into the dermis in the ear and the lateral expansion in the back skin. Dashed line, basement membrane. **c**,**f**, Immunofluorescence (left) and haematoxylin and eosin (H&E) (right) stainings of SmoM2-mutated cells in the ear (**c**) and back-skin (**f**) epidermis of K14Cre^{ER}/Rosa-SmoM2-YFP/Rosa-mT/mG mice at 12 and 24 weeks after tamoxifen induction. For H&E, dashed line: epidermal–dermal interface. **g**, Quantification of the vertical distance between WT and SmoM2 cells showing the depth of invasion of SmoM2-mutated clones at 2, 4 and 6 weeks after tamoxifen administration. Measurements of vertical invasion were performed from three mice for the ear and four mice for the back skin. **h**, Quantification of the lateral expansion of SmoM2-mutated clones in the ear and back-skin epidermis at 2, 4 and 6 weeks after tamoxifen administration ($n = 3$ mice for the ear and 4 mice for the back skin). **i**, Quantification of the number of cells per WT clone at 6 weeks after tamoxifen administration and the number of cells per SmoM2-expressing clone (total number of cells per clone) in the ear and back-skin epidermis at 2, 4 and 6 weeks after tamoxifen administration. Measurements of the clones were performed on the same image areas from two mice (SmoM2) and four mice (WT). Scale bars, 20 μm (**a**–**f**). **g**–**i**, The number of clones quantified is indicated in parentheses. Data are mean ± s.e.m. Kruskal–Wallis test.

assessed the fate of BrdU doublets, corresponding to the two daughter cells after division. In contrast with wild-type epidermis, which divided mostly asymmetrically, SmoM2 clones underwent symmetric renewing divisions (Extended Data Fig. 2j–l), in good accordance with the clonal analysis made by lineage tracing. These data show that clonal expansion in the ear epidermis after oncogenic SmoM2 expression switches rapidly from lateral expansion to vertical invasion.

To assess why oncogene expression in the back skin is not associated with BCC formation, we monitored the fate of oncogene-targeted cells over time in living mice using intravital microscopy. Of note, at first SmoM2-expressing cells in the back skin expanded laterally at the same rate as the epidermal cells of the ear epidermis. However, in sharp contrast to ear epidermis, oncogene-expressing cells in the back skin did not undergo a cell-shape transition and initiate downgrowth into the dermis, but instead continued to expand laterally (Fig. 1d,e,i). Even after six months after SmoM2 expression, oncogene-targeted cells continued to differentiate into suprabasal cells and presented a hyperplasia, resulting in a 'touch dome'-like morphology (Fig. 1f). Quantification of lateral spreading, invasion and clone size showed that, in contrast to wild-type cells targeted with a fluorescent protein, oncogene-targeted cells in the back-skin epidermis readily expanded after oncogene expression, leading to a similar clonal expansion and increase in self-renewing division to that observed in the ear epidermis; however, the clones expanded laterally and did not invade the dermis vertically (Fig. 1g–i). Similar to the ear epidermis, short-term BrdU pulse-chase experiments confirmed the switch from asymmetric division to symmetric renewal after SmoM2 expression (Extended Data Fig. 2j–l). These data show that the inability of the back-skin epidermis to undergo neoplastic transformation and invade the dermis after SmoM2 expression is not related to the inability of the oncogene-targeted stem cells to switch from an asymmetrical to a symmetrical mode of division, but is rather the consequence of their failure to switch from lateral expansion to vertical invasion.

Cell mechanics surrounding SmoM2 clones

As mutated clones expand over time, they must compete for the space with their wild-type neighbouring cells. Differences in cell mechanics between wild-type and oncogene-targeted cells can constrain the growth and expansion of mutated clones[18–20]. To assess the possible differences in mechanical properties of wild-type cells and mutant cells, we first quantified the shape of the cells at the interface of the mutated clone and wild-type cells over time. In the ear epidermis, wild-type cells at the border of the clones became deformed as shown by the increase in the aspect ratio of the cells (ratio of cell width to cell height) as soon as the mutated cloned adopted a placode-like morphology and before the mutated clone became invasive. The aspect ratio of the wild-type border cells in the ear further increased as the clones grew and became invasive. By contrast, in the back skin, no change in cell shape or aspect ratio was found in the wild-type cells contacting the mutated clones (Fig. 2a,b). These data suggest that in the ear epidermis, oncogene-targeted clones and wild-type border cells generate an interface exhibiting features of high interfacial tension that might restrain its lateral expansion and thus participate in promoting vertical growth. In the back skin, the wild-type cells at the border of the SmoM2-expressing clone were not elongated (Fig. 2b), indicating the absence of a specific mechanical interface in this tissue compartment.

To further define the role and source of the mechanical force exerted by the mutated clones on wild-type cells, we assessed the remodelling of the actomyosin cytoskeleton during the early step of tumour initiation. Phalloidin staining showed a major increase in the level of F-actin in oncogene-targeted cells in the ear as soon as SmoM2 cells adopted a placode-like shape. By contrast, no change in phalloidin staining was found in oncogene-targeted clones in the back-skin epidermis (Fig. 2c and Extended Data Fig. 3a–d). Immunostaining of

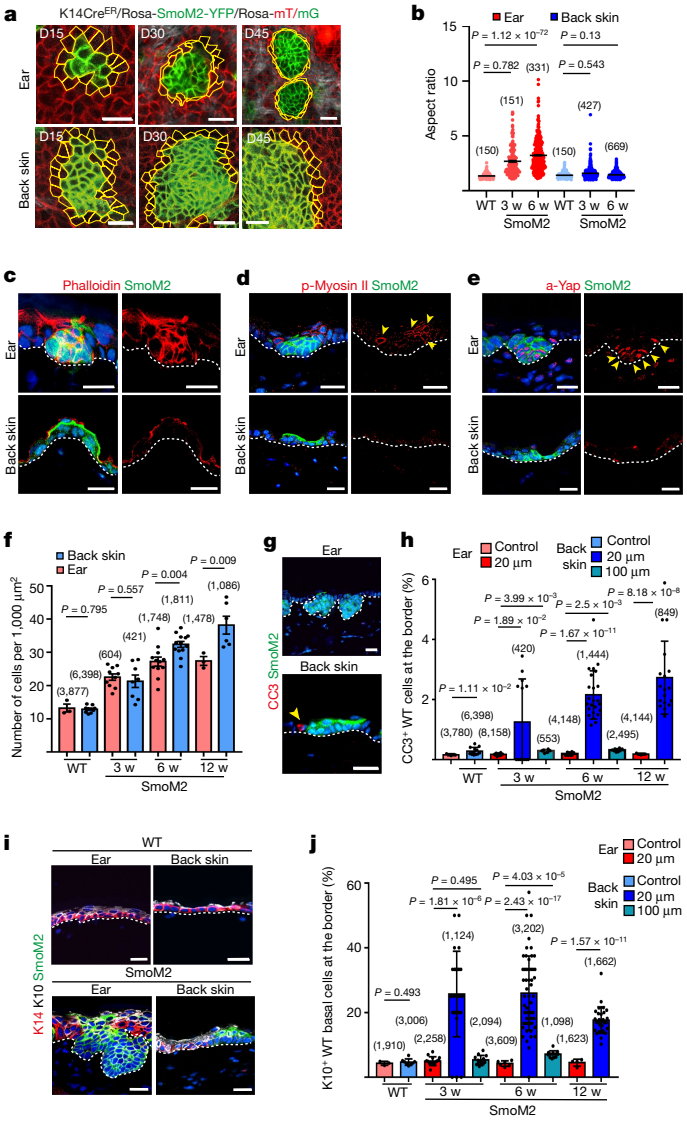

Fig. 2 | Difference in cell mechanics and competition in the ear and in the back-skin epidermis after SmoM2 expression. a, Intravital imaging showing the shape of WT cells at the border of SmoM2 clones in the ear and back-skin epidermis. WT cells become elongated in the ear, whereas they remain cuboidal in the back skin. **b**, Quantification of the aspect ratio of WT control cells ($n = 3$) and WT cells around SmoM2 clones at 3 weeks ($n = 4$) and 6 weeks ($n = 3$ for the ear and $n = 2$ for the back skin) after oncogenic expression. Mean ± s.e.m. Two-tailed z-test. **c**–**e**, Immunostaining for actin (**c**), phospho-myosin II (**d**) and active YAP (**e**) in K14Cre^{ER}/Rosa-SmoM2-YFP mice at 3 weeks after SmoM2 activation. Yellow arrowheads show phospho-myosin II-positive cells (**d**) and active-Yap-positive cells (**e**). **f**, Quantification of cell density in control ($n = 3$) and K14Cre^{ER}/Rosa-SmoM2-YFP mice at 3 weeks ($n = 3$), 6 weeks ($n = 5$) and 12 weeks ($n = 3$) after SmoM2 expression. Mean ± s.e.m. Paired t-test, with two-sample unequal variance. **g**, Immunostaining for cleaved caspase 3 (CC3) in K14Cre^{ER}/Rosa-SmoM2-YFP mice at 6 weeks after SmoM2 activation in the ear and back skin. Yellow arrowhead shows apoptotic cells. **h**, Quantification of WT apoptotic cells in controls ($n = 3$) and within 20 µm and 100 µm of SmoM2 clones in K14Cre^{ER}/Rosa-SmoM2-YFP mice at 3 weeks ($n = 3$), 6 weeks ($n = 4$) and 12 weeks ($n = 3$) after SmoM2 expression. **i**, Immunostaining for keratin 14 (K14) and K10 in K14Cre^{ER}/Rosa-SmoM2-YFP mice at 6 weeks after SmoM2 activation in the ear (left) and back skin (right). **j**, Quantification of WT K10$^+$ basal cells in controls ($n = 3$) and within 20 µm and 100 µm of SmoM2 clones in K14Cre^{ER}/Rosa-SmoM2-YFP mice at 3 weeks ($n = 3$), 6 weeks ($n = 3$ for the ear, $n = 5$ for the back skin at 20 µm and $n = 4$ at 100 µm) and 12 weeks ($n = 3$) after SmoM2 activation. **h**,**j**, Data are mean ± s.e.m. Kruskal–Wallis test. Scale bars, 20 µm (**a**,**c**–**e**,**g**,**i**). The number of clones quantified is indicated in parentheses. *n*, number of mice.

phosphorylated myosin light chain 2 revealed an increase in myosin activity in SmoM2-expressing cells and their wild-type neighbours at the border of oncogene-mutated clones in the ear epidermis but not in the back skin (Extended Data Fig. 3b). Quantification of YAP activity as a further indication of increased mechanical tension showed increased nuclear YAP at the leading edge of invading clones and in the wild-type neighbours at the border of clones, whereas only very occasional nuclear active-YAP-positive cells were found in the back-skin SmoM2-expressing clones (Fig. 2c,e). Collectively, these data indicate increased mechanical tension specifically at the clone boundary and enhanced cortical actin in the mutant cells in the ear, which explains their ability to laterally confine wild-type cells. These data are reminiscent of the role of compressive forces that trigger the downward migration of early hair follicles during embryonic development[21]. By contrast, oncogene-targeted cells in the back skin showed no evidence for mechanical-force-mediated cell competition between wild-type and oncogene-mutated cells at this body location.

Instead, in the back skin, the increase in the proliferation of SmoM2-mutated cells at the border of the clones was associated with a decrease in cell size and increase in cell density within the mutated clone, accompanied by an increase in the aspect ratio of the SmoM2-expressing cells at the centre of the clones (Fig. 2f and Extended Data Figs. 4a–e and 5c), indicative of mechanical confinement inside the clone. To assess in real time the cellular rearrangement of SmoM2-mutated clones in the back skin during clonal expansion, we performed live imaging of SmoM2-mutated clones over time for 54 h. We found that SmoM2-mutated clones progressively outcompeted their wild-type neighbours through specific patterns of cellular rearrangements, including progressive displacement, encirclement, intercalation and extrusion of wild-type cells (Extended Data Fig. 4f). This pattern of cell intercalation with no apparent sharp mechanical interface between wild-type and mutated clones suggests that SmoM2-mediated clonal expansion occurs through an active mechanism of cell competition independently of mechanical stress.

Cell competition induced by SmoM2

Several mechanisms of cell competition have been described, including mechanical cell competition, induction of apoptosis and cell differentiation[9,10,18,20,22]. To assess the nature of the active mechanisms that induce cell competition in the back skin after SmoM2 expression, we first determined whether SmoM2 clones can induce cell death at the border of the clones. In the ear epidermis, despite the compression of wild-type cells, there was no increase in the proportion of cleaved caspase 3 (CC3)-positive cells in wild-type basal cells at the border of the mutated clones, and $CC3^+$ cells were found mostly at the centre of the mutated clones, as previously described[14] (Fig. 2g and Extended Data Figs. 4g,h and 5a). By contrast, there was a substantial increase in the proportion of $CC3^+$ wild-type cells at the border of the SmoM2 clones in the back-skin epidermis (Fig. 2g,h), showing that SmoM2-expressing cells increase the apoptosis of wild-type cells in this skin region.

To assess whether, in addition to promoting cell death, oncogene-expressing cells outcompete their wild-type neighbouring cells by inducing their terminal differentiation[23], we quantified the expression of keratin 10 (K10), a differentiation marker, in wild-type basal cells ($K14^+$) at the border of SmoM2 clones. Whereas wild-type basal cells did not show increased differentiation in the ear epidermis, there was a major increase in the proportion of basal cells that expressed K10 at the border of SmoM2 clones in the back-skin epidermis, indicating that SmoM2-expressing cells induce the differentiation of their wild-type neighbours in the back skin (Fig. 2i,j and Extended Data Fig. 5b).

Altogether, these data show that SmoM2-expressing cells have an ability to compete with wild-type cells that differs depending on their location in the body, and that SmoM2 clones in the back skin are much more effective at inducing lateral cell competition than are those in the ear epidermis. This provides a plausible mechanism by which SmoM2-expressing cells can expand horizontally in the back skin without necessarily being associated with tumour invasion.

EHFP reprogramming induced by SmoM2

To uncover the molecular mechanisms by which the expression of SmoM2 in the ear leads to BCC initiation, whereas expressing the same oncogene in the back skin leads to a lateral clonal expansion that does not invade the dermis and lead to tumour formation, we performed a temporal analysis of single-cell RNA sequencing (RNA-seq) in wild-type and SmoM2-expressing basal cells of the back-skin and ear epidermis using 10X Chromium. We analysed the cells at three weeks after oncogene expression, when the first difference between the back-skin epidermis and the ear epidermis begins to be visible, and at six weeks, when the dermal invasion is well established in the ear. Unsupervised clustering of wild-type ear and back-skin epidermis showed similar clusters associated with the different cell states previously described[24–27] (Extended Data Fig. 6a–d). SmoM2-expressing basal cells showed the same clusters as well as the appearance of extra clusters corresponding to new cellular states expressing the molecular signature of EHFP reprogramming with high expression of *Lhx2* and *Lgr5* (Fig. 3a,c,e). The reprogramming of adult IFE stem cells into EHFP-like cells has previously been shown to be important for SmoM2-induced BCC formation in the tail epidermis[28,29]. The EHFP signature is associated with a higher level of Hedgehog (for example, *Ptch1*) and WNT (for example, *Wnt6*, *Fzd1*, *Lef1* and *Lgr5*) signalling, as well as higher expression of key genes that regulate the extracellular matrix (ECM) or basal lamina (for example, *Adamts1*, *Col14a1*, *Postn* and *Lama5*), cell–cell adhesion (for example, *Alcam* and *Cdh3* (encoding P-cadherin)), cell survival and proliferation (for example, *Mycn*) and cell migration (for example, *Sox9*), which are likely to participate in the dermal invasion (Extended Data Figs. 7a–g and 13a). By contrast, SmoM2-expressing basal cells in the back skin showed very similar clusters to the wild-type control, with a very small cluster (about 5%) expressing the EHFP signature and a higher proportion of cells associated with a differentiation program (expression of K1 and K10) (Fig. 3b,d,f).

Immunostaining confirmed the expression of EHFP genes in the SmoM2-expressing clones in the ear as soon as the SmoM2-expressing cells began to invade the dermis, and the highest expression of these EHFP-associated genes was found at the leading edge of the invasive tumours (Fig. 3g and Extended Data Fig. 8a,c), further supporting the notion that contact with the dermis regulates EHFP reprogramming. In the back skin, there were occasional small buds in contact with the dermis that expressed EHFP markers, but these cells never induced invasive tumours (Fig. 3h and Extended Data Fig. 8b,d). Altogether, these data show that SmoM2 expression differentially affects cellular reprogramming, resulting in new cell states induced by the oncogene in distinct regions of the skin, which in turn controls tumour initiation.

ECM in BCC-competent and BCC-resistant skin

To investigate whether a different composition of the dermis in the ear and the back skin affects the ability of oncogene-targeted cells to form BCC, we performed an unbiased quantitative proteomic analysis before and six weeks after oncogene expression. This analysis revealed that only a few proteins were more highly expressed in the back skin than in the ear, including COL1A1 and COL1A2 (Fig. 4a). RNA-fluorescence in situ hybridization (RNA-FISH) on skin sections confirmed that many more fibroblasts in the back-skin dermis expressed high levels of *Col1a1* and *Col1a2* as compared to the ear dermis (Fig. 4b). Multiphoton intravital imaging of the ear and back skin with second harmonic generation (SHG) revealed a very distinct organization of collagen fibres in the

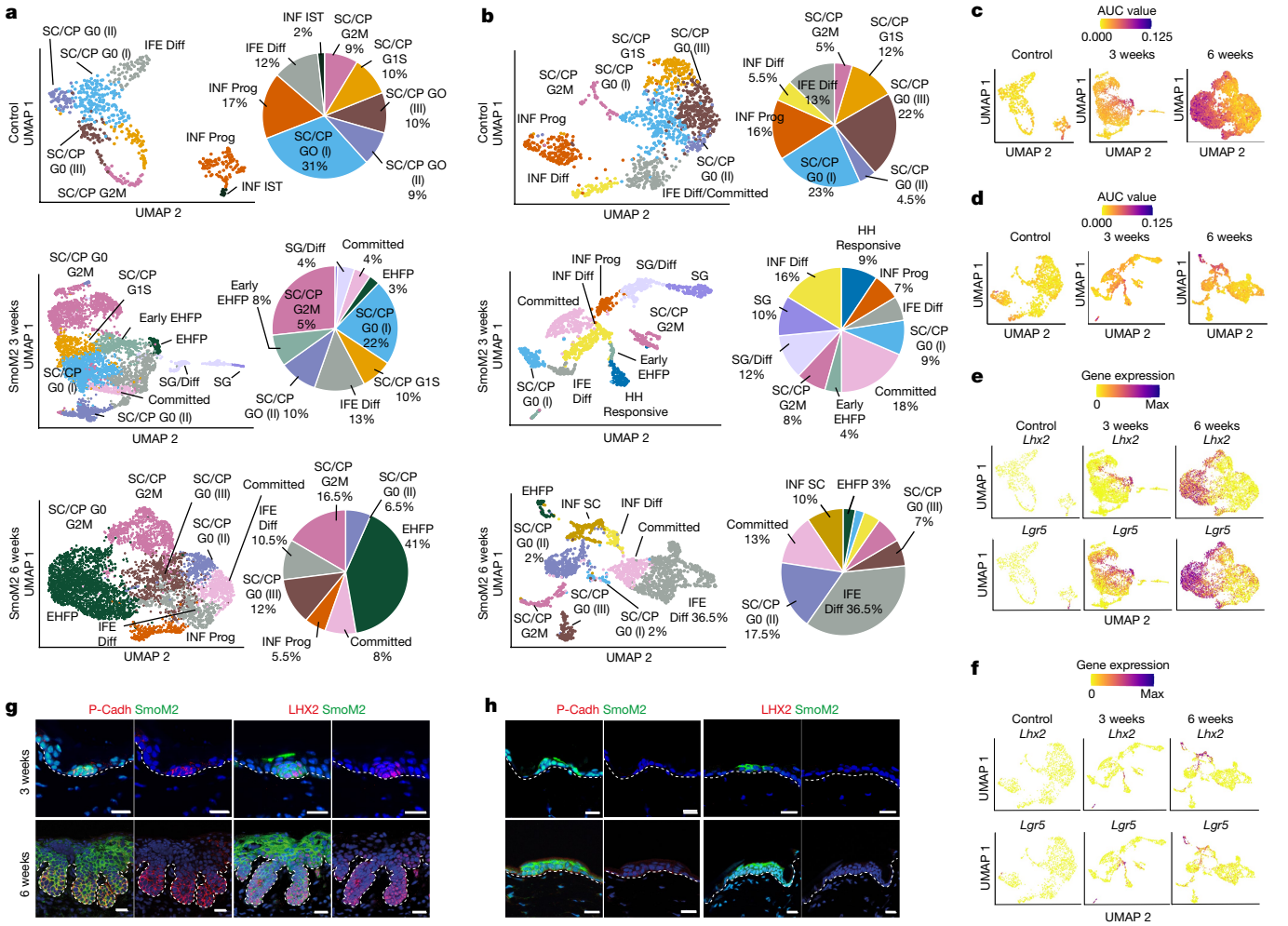

Fig. 3 | Single-cell RNA-seq reveals a block of oncogene-induced EHFP reprogramming in the back skin. a,**b**, Single-cell RNA-seq of WT and SmoM2-expressing cells from the back skin and ear at 3 and 6 weeks after oncogene expression. Left, uniform manifold approximation and projection (UMAP) of the unsupervised clustering analysis of single-cell RNA-seq of basal keratinocytes isolated from WT and 3 weeks and 6 weeks after SmoM2 expression in the ear (**a**) and the back skin (**b**). Right, pie charts representing the proportion of the different clusters in the different conditions. SC/CP, stem cell or committed progenitors; IFE Diff, interfollicular differentiated; INF Prog, infundibulum progenitors; INF IST, infundibulum isthmus; INF Diff, infundibulum differentiated; SG, sebaceous gland; HH Responsive, Hedgehog responsive. 'Committed cells' are basal cells committed to differentiation that express markers such as K14, K1 and HES1. **c**,**d**, UMAP plots showing the enrichment score of the EHFP signature[28,37] in each cellular cluster from control, 3-week and 6-week SmoM2-expressing cells isolated from the ear (**c**) and the back-skin epidermis (**d**). Colour scaling represents the area under the curve (AUC) score of EHFP enrichment as computed by AUCell. **e**,**f**, UMAP plots showing the normalized level of gene expression for the indicated EHFP genes (*Lhx2* and *Lgr5*) in the ear (**e**) and the back skin (**f**). Gene expression is visualized as a colour gradient. **g**,**h**, Immunostaining of ear (**g**) and back skin (**h**) for the EHFP marker P-cadherin, LHX2 and YFP in control and in K14Cre^{ER}/Rosa-SmoM2-YFP mice at 3 weeks and 6 weeks after SmoM2 expression. Scale bars, 20 µm.

different skin regions. Whereas the back-skin dermis was made up of abundant and thick collagen fibres, the ear dermis presented a much sparser collagen-fibre network (Fig. 4c–f and Extended Data Fig. 9a,b). Immunohistochemistry confirmed that collagen I was expressed much more abundantly in the dermis of the back skin than in the dermis of the ear skin, and that this pattern persisted after SmoM2 expression (Fig. 4g). Force indentation spectroscopy based on atomic force microscopy showed that the back-skin dermis was substantially stiffer than the ear dermis in wild-type and SmoM2 conditions (Fig. 4h). Together, these data show that there is a major difference in the composition and stiffness of the ECM between the ear skin and the back skin, suggesting that the higher expression of collagen I in the back skin is associated with the inability of oncogene-expressing cells to invade the dermis.

We have previously shown that the cellular composition of the dermis is remodelled in the tail-skin epidermis after SmoM2-induced BCC formation[28]. Consistent with this notion, a proteomic analysis of the dermis after SmoM2 expression showed that the ear dermis expressed many proteins associated with inflammation (such as S100a9 and MPO) (Extended Data Fig. 10a–c). As shown by H&E staining, the cellular infiltration of the ear dermis markedly increased after SmoM2 expression in the ear, whereas it remained unchanged in the back skin (Extended Data Fig. 8d). In the absence of oncogene expression, the relative abundance of immune and inflammatory cells (CD45$^+$, CD68$^+$, CD4$^+$ and CD8$^+$) within the dermis was relatively similar in the ear and back-skin epidermis (Extended Data Fig. 10d–f).

Collagen I constrains BCC development

Collagen immunostaining showed that the expression of collagen I was higher in the inner part of the ear than in the outer part of the ear, and there was an inverse correlation between the level of collagen I expression and the ability of SmoM2-expressing cells to invade the dermis (Fig. 5a–d). The tail epidermis is organized into two distinct

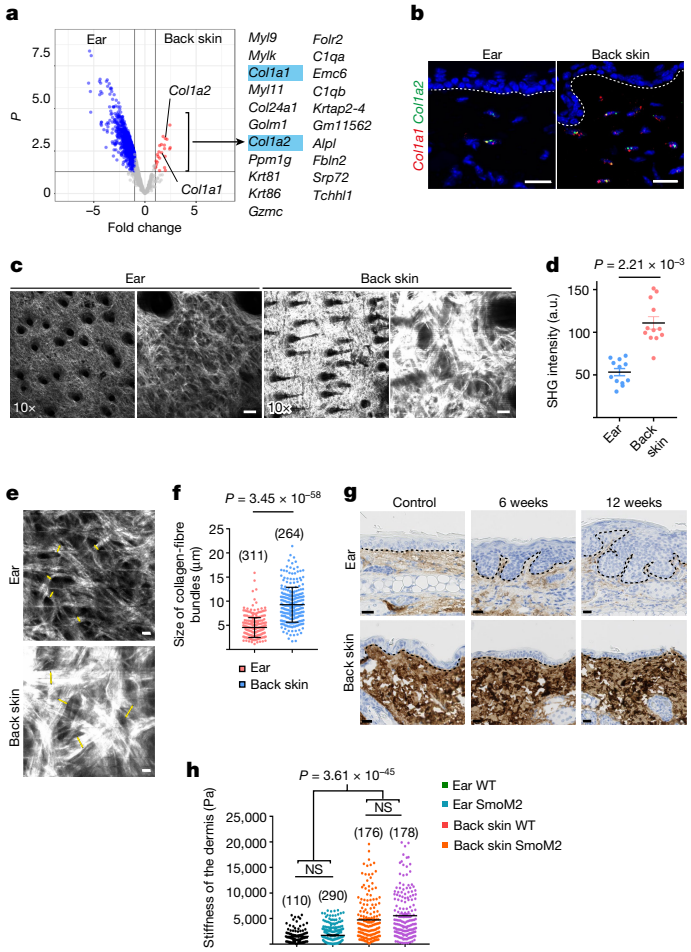

Fig. 4 | The level of collagen I expression correlates with the competence for BCC initiation. a, Quantitative proteomic analysis of WT dermis from the ear and the back skin. Volcano plot shows the significantly (false discovery rate (FDR) < 0.05 and log2(fold change)) upregulated proteins in the back skin and in the ear. **b**, RNA-FISH for *Col1a1* and *Col1a2* in the WT ear and back-skin dermis. **c**, SHG (fibrillar collagen) using confocal imaging of the ear and back-skin dermis in control mice. **d**, Quantification of the SHG intensities of ear and back-skin dermis in control mice. Measurements of SHG intensities were performed in three random areas using intravital microscopy ($n = 3$). a.u., arbitrary units. **e**, High magnification of the SHG using confocal imaging to assess collagen-fibre bundles in the ear and back-skin dermis in control mice. Yellow arrows indicate the size of collagen-fibre bundles. Scale bars, 5 μm. **f**, Quantification of the collagen bundle size in the WT ear and back skin ($n = 3$) using ImageJ. The number of bundles is shown in parentheses. **g**, Immunohistochemistry of collagen I in control and K14Cre^{ER}/Rosa-SmoM2-YFP mice at 6 and 12 weeks after SmoM2 activation. **h**, Stiffness of the dermis measured by atomic force microscopy. Quantification of the elastic modulus of the dermis in skin sections of the ear and back skin in control and K14Cre^{ER}/Rosa-SmoM2 mice 6 weeks after SmoM2 expression ($n = 2$ mice per condition). The number of measurements is shown in parentheses. NS, not significant. Scale bars, 20 μm (**b**,**c**,**g**). **d**,**f**,**h**, Data are mean ± s.e.m. Kruskal–Wallis test. *n*, number of mice.

regions: the scale and the interscale regions. In the tail epidermis, BCCs develop only from the interscale region whereas the SmoM2 clones in the scale remain blocked at the pre-neoplastic stage[14]. Notably, there was an excellent correlation between the level of collagen I expression and the ability of SmoM2 to induce BCC formation, further suggesting that the level of collagen I dictates the competence for tumour initiation (Extended Data Fig. 11a–d).

To assess whether the higher expression of collagen I restricts invasion and tumour formation in the back skin after SmoM2 expression, we enzymatically decreased the abundance of collagen and assessed how this affected tumour formation and invasion. To this end, we induced SmoM2 expression and, two weeks later, we subcutaneously injected collagenase twice per week in the back skin and measured invasion and tumour formation six weeks after tamoxifen administration. Collagenase injections rapidly decreased the abundance and density of collagen fibres (Fig. 5e,f). After the administration of collagenase in control mice, an invasion of epidermal cells into the dermis was not observed and the basal lamina was unaffected (Extended Data Fig. 12a–c). However, decreasing the abundance and thickness of the collagen bundles without impairing their orientation in the back skin by collagenase injection overcame the resistance of the back skin to SmoM2 transformation and led to the development of tumorigenic lesions that invaded the dermis. These invasive lesions begun to express EHFP markers similarly to SmoM2 tumours that grow spontaneously in the ear and tail skin (Fig. 5e–i and Extended Data Fig. 9c–f). To assess whether the inflammation associated with collagenase administration could promote invasion by itself, we induced inflammation and assessed whether this induced the dermal invasion of SmoM2 clones. Whereas bleomcyin or imiquimod induced strong inflammation in the dermis, they did not promote the invasion of the SmoM2 cells in the back skin, showing that inflammation is not sufficient to promote BCC formation (Extended Data Fig. 12d–i).

It has previously been shown that ageing is associated with a decrease in collagen density in the skin[30,31]. We therefore assessed the collagen density by immunohistochemistry and confocal microscopy using SHG in aged mice. Our analysis showed that the level of collagen markedly decreased in mice that were older than 1.5 years. To assess whether the decrease in collagen density associated with ageing promotes the ability of the back-skin epidermis to undergo tumorigenesis, we induced the expression of oncogenic SmoM2 in 1.5-year-old mice and analysed BCC formation six weeks after oncogene expression. Of note, SmoM2-expressing cells invaded the dermis of the back skin of aged mice, and this invasion was associated with EHFP reprogramming (Fig. 5j–o,s). Moreover, we found that in aged mice, there was a decrease in lateral expansion concomitant with an increase in the vertical invasion of the clones (Fig. 5t,u). The decrease in the lateral expansion was associated with a decrease in the ability of SmoM2-expressing cells to promote the terminal differentiation of the wild-type border cells in the back skin (Fig. 5v). These data reveal the balance between lateral expansion and vertical outgrowth after SmoM2 expression and further reinforce the notion that the level of collagen expression dictates the competence for BCC initiation.

UV exposure is also well known to decrease collagen expression[32]. UVB rays are absorbed by the epidermis, whereas UVA rays penetrate to the dermis and induce premature ageing of the skin and reduced collagen I expression[33]. To assess whether the decrease in collagen expression after chronic UVA exposure promotes the formation of BCC, we irradiated the back skin of the mice using a UVA lamp five times per week for a total of ten weeks[34]. At the end of the fourth week, we induced SmoM2 expression and assessed the expression of collagen I and the formation of BCC. Chronic UVA exposure led to a strong reduction in the level of collagen I. Notably, the decrease in collagen I expression induced by chronic UVA exposure was associated with the ability of SmoM2-expressing cells in the back skin to lead to BCC formation and invasion as well as EHFP reprogramming (Fig. 5j–l,p–s). The complete penetrance of the invasion phenotype in the back skin after UVA administration suggests that random secondary mutations are not likely to be the driving force of tumour invasion. Altogether, these data indicate that the high levels of collagen I expression in the dermis are responsible for the natural resistance of the back-skin epidermis to forming BCC after SmoM2 expression, and suggest that the contact of oncogene-expressing cells with the dermal microenvironment is important for the EHFP reprogramming of these cells during tumour initiation.

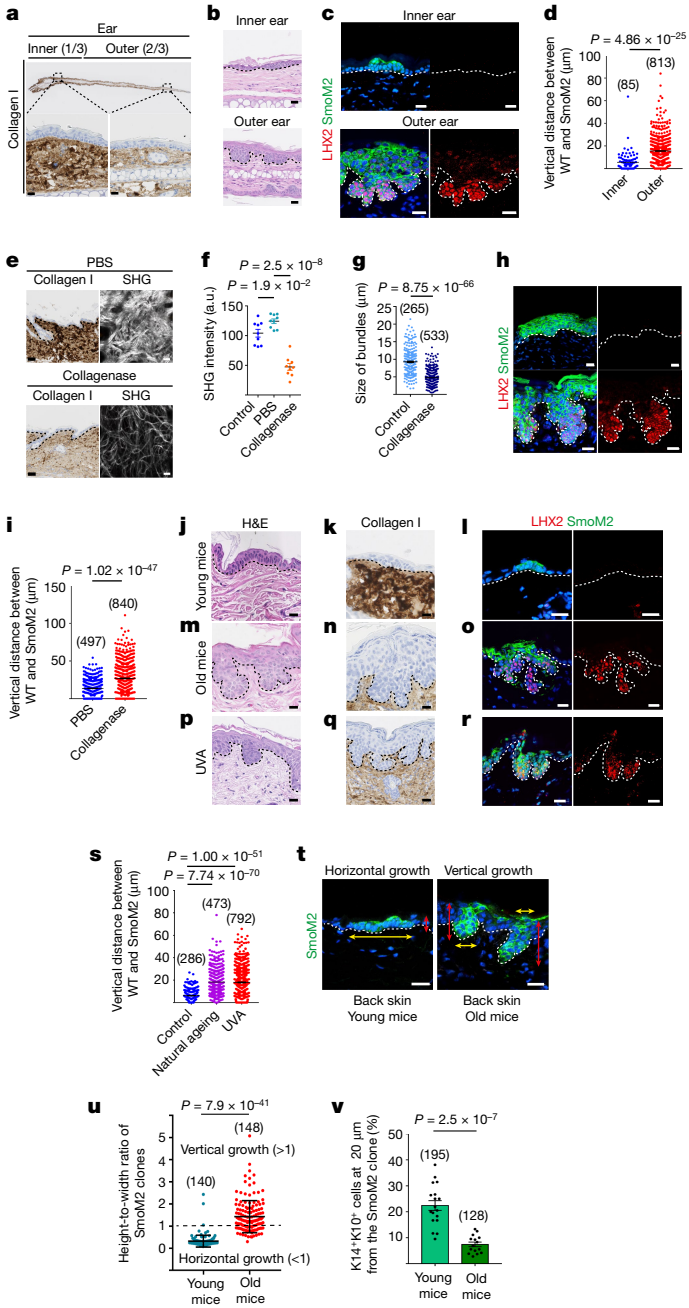

Fig. 5 | High levels of collagen I expression constrain BCC development. **a**, Collagen I immunohistochemistry in the inner and outer ear. **b**,**c**, H&E staining (**b**) and immunostaining of LHX2 (**c**) in the ear of K14Cre^{ER}/Rosa-SmoM2-YFP mice at 6 weeks after SmoM2 activation. **d**, Quantification of tumour invasion measured by the vertical distance between WT cells and SmoM2 cells in the ear at 6 weeks after SmoM2 activation ($n = 4$). **e**,**f**, Collagen I immunohistochemistry for collagen I and confocal analysis using SHG (**e**) and SHG quantification (**f**) of the back-skin dermis before and one day after intradermal injection of phosphate-buffered saline (PBS) or collagenase. Scale bars, 50 μm (immunohistochemistry); 20 μm (SHG). Measurements of SHG intensities were performed on three random areas ($n = 4$ mice). **g**, Quantification of the collagen bundle size in WT back skin and in back skin after collagenase injection ($n = 3$ mice). **h**, LHX2 immunostaining in the back skin after injection of collagenase or PBS 6 weeks after SmoM2 expression. **i**, Vertical distance between WT cells and SmoM2 cells at 6 weeks after SmoM2 expression in the back skin after injection of collagenase or PBS ($n = 6$ mice.) **j**–**r**, H&E staining (**j**,**m**,**p**), collagen I immunohistochemistry (**k**,**n**,**q**) and LHX2 and SmoM2 immunostaining (**l**,**o**,**r**) of the back skin in SmoM2 young (**j**–**l**), 1.5-year-old (**m**–**o**) and UVA-treated (**p**–**r**) mice. **s**, Vertical distance between WT cells and SmoM2 cells 6 weeks after the administration of tamoxifen in the back skin of control mice ($n = 3$), old mice ($n = 2$) and mice treated with UVA for 8 weeks ($n = 6$). **t**, Immunostaining of SmoM2 clones of the back skin in young (left) and 1.5-year-old (right) SmoM2 mice 6 weeks after SmoM2 expression. Yellow arrows, width; red arrows, height. **u**, Ratio between the height and width of SmoM2 clones in the back skin in SmoM2 young ($n = 3$) and old ($n = 2$) mice 6 weeks after SmoM2 expression. Mean ± s.e.m. Two-tailed z-test. **v**, Quantification of WT basal cells expressing K10 at 20 μm around SmoM2 clones in the back skin in young ($n = 3$) and 1.5-year-old ($n = 2$) mice 6 weeks after SmoM2 expression. Mean ± s.e.m. Paired t-test, with two-sample unequal variance (heteroscedastic). **a**,**d**,**f**,**g**,**i**,**s**, Data are mean ± s.e.m. Kruskal–Wallis test. Scale bars, 20 μm (**a**–**c**,**h**,**j**–**r**,**t**.). The number of clones (**d**,**i**,**s**,**u**,**v**) or measurements (**g**) is shown in parentheses.

Discussion

In this study, we use intravital microscopy to track and follow the same cells expressing the SmoM2 oncogene over time in living animals, from the first targeted cell until the development of invasive tumours. We show that not all epidermal cells across the body are equally sensitive to oncogenic transformation after SmoM2 expression. Whereas the ear epidermis is susceptible to oncogenic transformation, the back skin is profoundly resistant. Although the extent of clonal expansion is similar between the two tissues, the oncogene-targeted clones expand and compete with the wild-type basal cells by promoting their apoptosis and terminal differentiation in a lateral manner without invading the dermis. The finding that oncogene-induced cell competition does not necessarily lead to tumour initiation could explain why mutated clones for cancer drivers can be found in normal human tissues without any signs of neoplastic transformation[13,35]. By contrast, in the ear epidermis, after a short phase of lateral expansion, the oncogene-targeted clones begin to grow downwards and invade the dermis. The switch between lateral and vertical growth and the early steps of tumour invasion are associated with a reprogramming of the adult IFE stem cells into an EHFP-like fate that is essential for BCC initiation[28,29] (Extended Data Fig. 14).

Our data reveal that only the susceptible part of the skin, and not the resistant back-skin epidermis, undergoes this EHFP reprogramming after oncogene expression. We show that the resistance to oncogene transformation is dictated by the stiffness of the dermis and the composition of the ECM. These data are consistent with a previous study showing that in embryonic development, during which collagen expression is almost absent[36], the remodelling of a soft basal lamina promotes BCC formation[17]. Decreases in the concentration of collagen as a consequence of collagenase injection, chronic UVA exposure or natural ageing rescue the ability of oncogene-expressing cells in the back skin to undergo tumour invasion, EHFP reprogramming of oncogene-expressing cells and BCC formation, providing evidence that these key features are dictated by the contact between oncogene-expressing cells and the ECM of the deeper dermis. These data are relevant for human skin cancer, for several reasons. First, BCC also tends to arise preferentially in certain locations of the human body; for example, it is more common in the ear and the nose than in the cheek, despite the fact that the cheek has a larger surface area and is exposed to similar levels of UV. Second, analogous to the effect of UVA in mice, chronic sun exposure is one of the most important risk factors for BCC formation in humans. And finally, similarly to what is observed in aged mice, BCC frequently develops in older humans.

Further studies will be required to investigate the relevance of these findings for constraining or promoting clonal cell competition and tumour development in the different tissues that contain mutations in cancer-driver genes[8]. Our results also have implications for understanding the cellular non-autonomous factors that have a key role in tumour initiation, and identifying the cells in a tissue that are susceptible to undergoing neoplastic transformation.

Online content

Any methods, additional references, Nature Portfolio reporting summaries, source data, extended data, supplementary information, acknowledgements, peer review information; details of author contributions and competing interests; and statements of data and code availability are available at https://doi.org/10.1038/s41586-023-06740-y.

1. Blanpain, C. & Fuchs, E. Epidermal stem cells of the skin. *Annu. Rev. Cell Dev. Biol.* **22**, 339–373 (2006).
2. Hsu, Y. C. & Fuchs, E. Building and maintaining the skin. *Cold Spring Harb. Perspect. Biol.* **14**, a040840 (2022).
3. Blanpain, C. & Simons, B. D. Unravelling stem cell dynamics by lineage tracing. *Nat. Rev. Mol. Cell Biol.* **14**, 489–502 (2013).
4. Epstein, E. H. Basal cell carcinomas: attack of the hedgehog. *Nat. Rev. Cancer* **8**, 743–754 (2008).
5. Kasper, M., Jaks, V., Hohl, D. & Toftgard, R. Basal cell carcinoma—molecular biology and potential new therapies. *J. Clin. Invest.* **122**, 455–463 (2012).
6. Youssef, K. K. et al. Identification of the cell lineage at the origin of basal cell carcinoma. *Nat. Cell Biol.* **12**, 299–305 (2010).
7. Mao, J. et al. A novel somatic mouse model to survey tumorigenic potential applied to the Hedgehog pathway. *Cancer Res.* **66**, 10171–10178 (2006).
8. Di Gregorio, A., Bowling, S. & Rodriguez, T. A. Cell competition and its role in the regulation of cell fitness from development to cancer. *Dev. Cell* **38**, 621–634 (2016).
9. Merino, M. M., Levayer, R. & Moreno, E. Survival of the fittest: essential roles of cell competition in development, aging, and cancer. *Trends Cell Biol.* **26**, 776–788 (2016).
10. Levayer, R. Solid stress, competition for space and cancer: the opposing roles of mechanical cell competition in tumour initiation and growth. *Semin. Cancer Biol.* **63**, 69–80 (2020).
11. Moreno, E. & Basler, K. dMyc transforms cells into super-competitors. *Cell* **117**, 117–129 (2004).
12. de la Cova, C., Abril, M., Bellosta, P., Gallant, P. & Johnston, L. A. *Drosophila* Myc regulates organ size by inducing cell competition. *Cell* **117**, 107–116 (2004).
13. Kakiuchi, N. & Ogawa, S. Clonal expansion in non-cancer tissues. *Nat. Rev. Cancer* **21**, 239–256 (2021).
14. Sanchez-Danes, A. et al. Defining the clonal dynamics leading to mouse skin tumour initiation. *Nature* **536**, 298–303 (2016).
15. Mascre, G. et al. Distinct contribution of stem and progenitor cells to epidermal maintenance. *Nature* **489**, 257–262 (2012).
16. Clayton, E. et al. A single type of progenitor cell maintains normal epidermis. *Nature* **446**, 185–189 (2007).
17. Fiore, V. F. et al. Mechanics of a multilayer epithelium instruct tumour architecture and function. *Nature* **585**, 433–439 (2020).
18. Levayer, R., Dupont, C. & Moreno, E. Tissue crowding induces caspase-dependent competition for space. *Curr. Biol.* **26**, 670–677 (2016).
19. Tsuboi, A. et al. Competition for space is controlled by apoptosis-induced change of local epithelial topology. *Curr. Biol.* **28**, 2115–2128 (2018).
20. Moreno, E., Valon, L., Levillayer, F. & Levayer, R. Competition for space induces cell elimination through compaction-driven ERK downregulation. *Curr. Biol.* **29**, 23–34 (2019).
21. Villeneuve, C. et al. Mechanical forces across compartments coordinate cell shape and fate transitions to generate tissue architecture. Preprint at *bioRxiv* https://doi.org/10.1101/2022.12.12.519937 (2022).
22. van Neerven, S. M. & Vermeulen, L. Cell competition in development, homeostasis and cancer. *Nat. Rev. Mol. Cell Biol.* **24**, 221–236 (2023).
23. Sandoval, M., Ying, Z. & Beronja, S. Interplay of opposing fate choices stalls oncogenic growth in murine skin epithelium. *eLife* **10**, e54618 (2021).
24. Aragona, M. et al. Defining stem cell dynamics and migration during wound healing in mouse skin epidermis. *Nat. Commun.* **8**, 14684 (2017).
25. Dekoninck, S. et al. Defining the design principles of skin epidermis postnatal growth. *Cell* **181**, 604–620 (2020).
26. Joost, S. et al. Single-cell transcriptomics reveals that differentiation and spatial signatures shape epidermal and hair follicle heterogeneity. *Cell Syst.* **3**, 221–237 (2016).
27. Joost, S. et al. Single-cell transcriptomics of traced epidermal and hair follicle stem cells reveals rapid adaptations during wound healing. *Cell Rep.* **25**, 585–597 (2018).
28. Youssef, K. K. et al. Adult interfollicular tumour-initiating cells are reprogrammed into an embryonic hair follicle progenitor-like fate during basal cell carcinoma initiation. *Nat. Cell Biol.* **14**, 1282–1294 (2012).
29. Yang, S. H. et al. Pathological responses to oncogenic Hedgehog signaling in skin are dependent on canonical Wnt/beta3-catenin signaling. *Nat. Genet.* **40**, 1130–1135 (2008).
30. Pieraggi, M. T., Julian, M. & Bouissou, H. Fibroblast changes in cutaneous ageing. *Virchows Arch. A Pathol. Anat. Histopathol.* **402**, 275–287 (1984).
31. Salzer, M. C. et al. Identity noise and adipogenic traits characterize dermal fibroblast aging. *Cell* **175**, 1575–1590 (2018).
32. Lan, C. E., Hung, Y. T., Fang, A. H. & Ching-Shuang, W. Effects of irradiance on UVA-induced skin aging. *J. Dermatol. Sci.* **94**, 220–228 (2019).
33. Wlaschek, M. et al. Solar UV irradiation and dermal photoaging. *J. Photochem. Photobiol. B* **63**, 41–51 (2001).
34. Kligman, L. H. The hairless mouse model for photoaging. *Clin. Dermatol.* **14**, 183–195 (1996).
35. Martincorena, I. et al. High burden and pervasive positive selection of somatic mutations in normal human skin. *Science* **348**, 880–886 (2015).
36. Rognoni, E. et al. Fibroblast state switching orchestrates dermal maturation and wound healing. *Mol. Syst. Biol.* **14**, e8174 (2018).
37. Rhee, H., Polak, L. & Fuchs, E. Lhx2 maintains stem cell character in hair follicles. *Science* **312**, 1946–1949 (2006).

Methods

Mice

Mouse colonies were housed and maintained in a certified animal facility in accordance with the European guidelines. All animal procedures were approved by the corresponding ethical committee (Commission d'Ethique et du Bien Être Animal (CEBEA), Faculty of Medicine, Université Libre de Bruxelles) under protocol numbers 794 and 820. CEBEA follows the European Convention for the Protection of Vertebrate Animals used for Experimental and other Scientific Purposes. This study complies with all ethical regulations regarding animal research. Mice were monitored daily and euthanized when tumours became macroscopic, if the skin was ulcerated or haemorrhagic or if the mouse lost more than 20% of its initial weight or showed any other sign of distress (on the basis of general health and spontaneous activity). All of the experiments complied strictly with the protocols approved by the ethical committee. The housing conditions of all mice strictly followed the ethical regulations. The room temperature ranged from 20 to 24 °C. The relative ambient humidity at the level of mouse cages was 55 ± 10%. Each cage was provided with food, water and two types of nesting material. A semi-natural light cycle of 12:12 was used.

Mouse strains

The K14Cre^{ER} transgenic mouse model was generated and provided by the laboratory of E. Fuchs. This mouse model is available at the Jackson Laboratory, stock 005107. The Rosa26-LSL-SmoM2-YFP mouse line was imported from the Jackson Laboratory (stock 005130). The Rosa26-LSL-mT/mG mouse line was imported from the Jackson Laboratory (stock 07576). The iChr2-Control-Mosaic was provided by the laboratory of R. Benedito and is now available in the Jackson Laboratory (stock 031302). The mice used in this study were a mixture of males and females with mixed genetic backgrounds.

Inducing oncogene activation

Mice were induced between 1.5 and 4 months of age (apart from the experiment on old mice) with tamoxifen (Sigma-Aldrich) dissolved in 10% ethanol and 90% sunflower oil (Sigma). The quantity of tamoxifen administered to mice was adjusted in accordance with their weight. For non-clonal induction, mice were treated with a single intraperitoneal injection of tamoxifen at a dosage of 1 mg per 30 g. For clonal induction, mice were treated with a single intraperitoneal injection of tamoxifen at a dosage of 0.075 mg per 30 g (ear skin clonal dose) or 0.4 mg per 30 g (back skin clonal dose). Mice were euthanized at different time points after induction.

In vivo lineage tracing and imaging

Mice were first anaesthetized with vaporized isoflurane delivered in a box at 4% isoflurane + 2% oxygen. Then, they were placed into the microscope and maintained under anaesthesia by a nose cone delivering isoflurane at 2% isoflurane + 0.3% oxygen throughout the course of imaging sessions. The temperature inside the microscope was set at 29 °C to avoid hypothermia. Before the start of each experiment, the ear skin and back skin were shaved using clippers and depilatory cream. To navigate back to the same field of view and follow the behaviours of the same epidermal clones over multiple days, tattoos and inherent landmarks of the skin such as hair-follicle distribution were used. The ear skin was tattooed using a small needle and carbon ink as described previously[38]. The back skin was tattooed using a tattoo machine. Images were acquired on an LSM 880 confocal (Zeiss) fitted on a AxioObserver Z NLO inverted microscope (Zeiss). Multiphoton excitation from a tunable InSight X3 laser (Spectra Physics) was set at 920 nm to image SHG, GFP and dtTomato using emission filters (Chroma) KP 475 nm, BP 510–540 nm and BP 580–640 nm, respectively, in front of GaAsP non-descanned detectors (NDD) (Zeiss). Serial optical sections were acquired through a 40× dry lens (Zeiss) with a 0.6–1 µm step to image the entire thickness of the epidermis, invasion of the dermis by BCC and a part of the ECM thanks to the second harmonic signal.

Quantification of SHG intensity

Measurements of the intensity of SHG were analysed manually in ImageJ software. For the intensity of SHG, we analysed three random areas at 40× magnification for the ear and for the back skin from four different mice. The analysed area was defined manually to exclude hair follicles.

Measurements of the aspect ratio of epidermal cells

Measurements of the aspect ratio were performed manually using ImageJ software.

Measurements of collagen-fibre bundles

Measurements of collagen-fibre bundles were analysed manually in ImageJ software. For that, we measured at least 311 bundles for the ear, 263 bundles for the back skin and 533 bundles for the back skin with collagenase from 3 random areas at 40× magnification from 3 different mice.

Measurements of the orientation of collagen-fibre bundles

For the orientation of the collagen-fibre bundles, we used the plug-in OrientationJ in ImageJ to generate the hue-saturation-brightness (HSB) colour code and the histogram of local angles. Orientations are automatically calculated according to the collagen-fibre bundles and are represented as colour images with the orientation encoded in an HSB map. We analysed three random areas at 40× magnification for the wild-type ear, the wild-type back skin and the back skin with collagenase from three different mice.

Immunofluorescence of tissue sections

After dissection, samples of ear skin and back skin were embedded without prior fixation into optimal cutting temperature compound (OCT, Sakura), frozen on dry ice and kept at −80 °C. Tissues were then cut into 6–10 µm sections using a CM3050S Leica cryostat (Leica Microsystems). For immunostainings, frozen sections were dried for a few minutes at room temperature, fixed in 4% paraformaldehyde (PFA) for 10 min at room temperature and washed three times in PBS before being incubated with a blocking buffer (5% horse serum, 1% BSA and 0.2% Triton X-100) for one hour at room temperature. Sections were then incubated with primary antibodies diluted into blocking buffer, overnight at 4 °C. The day after, sections were washed three times in PBS and then incubated with secondary antibodies diluted at 1:400 and Hoechst (10 mg ml^{-1}) diluted at 1:2,000 in blocking buffer for one hour at room temperature. Sections were finally rinsed three times (5 min) in PBS and mounted in DAKO mounting medium supplemented with 2.5% Dabco (Sigma). The following primary antibodies were used: anti-GFP (goat polyclonal; Abcam, ab6673; 1:1,000), anti-GFP (rabbit polyclonal; Abcam, ab6556; 1:2,000), anti-CD104/β4 integrin (rat; BD Biosciences, 346-11A; 1:200); anti-K10 (rabbit; Covance, 905404; 1:2,000); anti-K1 (rabbit, Covance; 1:4,000), anti-K15 (chicken; Covance, 833904; 1:15,000); anti-LHX2 (goat; Santa Cruz, sc-19344; 1:500); anti-LEF1 (rabbit, Cell Signaling Technology, 2230; 1:200); anti-P-cadherin (rat; Invitrogen, 32000Z; 1:1,000); anti-vimentin (rabbit; Abcam, 92547; 1:1,000); anti-CD45 (rat; BD Biosciences, 103106; 1:50), anti-CD68 (rabbit; Abcam, ab125212; 1:1,000), anti-CD8 (rabbit; Abcam, ab203035; 1:200), anti-CD4 (rat; Biolegend, 100412; 1:200), anti-K14 (chicken, Thermo Fisher Scientific, MA5-11599, 1:2,000), anti-active YAP1 (rabbit; Abcam, ab205270; 1:200), anti-phospho-myosin light chain 2 (rabbit; Cell Signaling Technology, 3674S; 1:200), phalloidin (Invitrogen, A22287; 1:400), EdU (Thermo Fisher Scientific, c10340), anti-CC3 (rabbit; R&D, AF835; 1:400) and anti-lamin 5 (rabbit; Abcam, ab14509; 1:200). The following secondary antibodies were used (dilution 1:400): anti-rabbit, anti-rat, anti-chicken and anti-goat conjugated either to

Alexa Fluor 488 (Molecular Probes) or Rhodamine Red-X (Jackson ImmunoResearch) or cyanine 5 (Cy5) (Jackson ImmunoResearch). All confocal images from whole-mount epidermis were acquired at room temperature with a LSM780 confocal system fitted on an AxioExaminer Z1 upright microscope equipped with a C-Apochromat 40×/1.1 water objective.

RNA-FISH

Ear and back skin were dissected from the SmoM2 YFP and control mice, embedded in OCT (Sakura) and cut into 5–8-µm frozen sections using a CM3050S Leica cryostat (Leica Microsystems). Sections were fixed for 30 min in 4% PFA at 4 °C and the in situ protocol was performed according to the manufacturer's instructions (Advanced Cell Diagnostics). The following mouse probes were used: Mm-Col1a1 (319371) and Mm-Col1a2 (585461-C2).

Histology and immunohistochemistry

Ear-auricle and back-skin samples were fixed for 24 h in 10% neutral buffered formalin and routinely embedded in paraffin wax. Four-millimetre-thick sections were placed on Superfrost glass microscope slides (Gerhard Menzel) or Flex IHC microscope slides (Dako Agilent Technologies) and dried at 37 °C. Immunohistochemistry for the detection of collagen I was performed using a rabbit monoclonal antibody (Abcam ab270993, 1:1,000) on a Dako Autostainer Link 48 (Dako, Agilent Technologies). In brief, deparaffinized and hydrated tissue sections were treated with H_2O_2 3% for 5 min to quench endogenous peroxidase and incubated at 97 °C in EDTA buffer (pH 9.0) for 5 min for antigen retrieval. Tissue sections were incubated for 40 min with the primary antibody, washed and incubated for 20 min with FLEX immunoperoxidase polymer anti-rabbit IgG (Agilent). Immunolabelling was visualized by incubation with diaminobenzidine and hydrogen peroxide for 10 min and counterstaining with haematoxylin. The slides were digitized using the slide scanner Nanozoomer 2.0-HT (Hamamatsu) and analysed using QuPath (v.0.3.2).

Epidermal whole-mount immunostaining

The ear and the back skin were dissected from the experimental and control mice, cut into small pieces and incubated in 20 mM PBS-EDTA on a rocking plate at 37 °C for 1 h. The epidermis was separated from the dermis using forceps. Samples were washed twice with 1× PBS and then fixed in 4% PFA for 1 h at room temperature. They were then washed three times with 1× PBS for 5 min each wash and then stored in PBS and sodium azide (0.2%) at 4 °C. For immunofluorescence staining, we used the pieces of epidermal sheet, incubated in blocking buffer (1% BSA, 5% horse serum, 0.8% Triton in 1× PBS) for 3 h at room temperature on rocking plate. For primary antibody staining, samples were incubated with the primary antibodies anti-integrin β4 (rat, 1:200, BD Biosciences), K14 (1:2,000), K10 (1:1,000), anti-CC3 (1:600), anti-active YAP1 (1:200) and phalloidin (1:200) overnight at room temperature on a rocking plate (100 rpm). Samples were then washed three times with PBS 0.2% Tween for 20 min each and then incubated with secondary antibody and Hoechst (1:2,000) for nuclear staining for 2 h at room temperature on a rocking plate. Samples were washed three times with PBS 0.2% Tween for 20 min each and then mounted in DAKO mounting medium by keeping the hairy side down. For BrdU staining, epidermal sheets were incubated in 1 M HCl at 37 °C for 45 min and then washed with 1× PBS three times for 10 min each. Overnight incubation was performed with primary antibody anti-BrdU (rat, 1:200, Abcam) in blocking buffer at room temperature on a rocking plate. The next day, samples were washed three times with PBS 0.2% Tween for 20 min each and then incubated with secondary antibody and Hoechst (1:500) for 2 h at room temperature on a rocking plate. Samples were washed three times with PBS 0.2% Tween for 20 min each and then mounted in DAKO mounting medium by keeping the hairy side down. EdU staining was performed according to the manufacturer's instructions (Thermo Fisher Scientific). For co-expression with EdU, the K14 or other primary antibody staining was performed first, and then the EdU protocol was followed.

Proliferation experiments

For proliferation experiments, mice were injected with a single intraperitoneal injection of EdU (2.5 mg ml^{-1} in PBS) 4 h before euthanasia. We performed EdU staining as recommended by the manufacturer. For the quantification, an area of at least 1.5 mm per mouse was analysed with Zen2012 (Black Edition) software (Zeiss) to determine the percentage of EdU-positive cells.

Cell-fate divisions

To understand the dynamics of cell fate in the expansion of SmoM2 cells in the ear as well as the back skin, we performed a BrdU pulse-chase assay, which allows us to assess the fate of the divisions[14,39]. Mice were injected with a single intraperitoneal dose of BrdU (1.25 µg $µl^{-1}$) 24 h before euthanasia to capture the doublets of BrdU. We analysed BrdU doublets with SmoM2–YFP, with the location of BrdU in the basal–basal, basal–suprabasal or suprabasal–suprabasal position.

Liquid chromatography–tandem mass spectrometry analysis

Ear and back skin of CD1 mice and $K14Cre^{ER}$/Rosa-SmoM2-YFP (200 mg wet weight) were snap-frozen in liquid nitrogen and crushed using a mortar and pestle to obtain powder tissue. Three mice were used for each condition (wild type and SmoM2). For each sample, 10–70 mg skin or ear tissue was transferred to 1.5-ml tubes and 50 µl lysis buffer containing 5% sodium dodecyl sulfate (SDS) and 50 mM triethylammonium bicarbonate (TEAB, pH 8.5) was added. The samples were mechanically disrupted by two cycles of grinding with a disposable micropestle and heating to 90 °C in between cycles. Another 50 µl lysis buffer was added, and the resulting lysate was transferred to a 96-well PIXUL plate and sonicated with a PIXUL multisample sonicator (Active Motif) for 60 min with default settings (pulse 50 cycles, PRF 1 kHz, burst rate 20 Hz). After centrifuging the samples for 5 min at 2,204*g* and room temperature to remove insoluble components, the protein concentration was measured by bicinchoninic acid (BCA) assay (Thermo Fisher Scientific), and 300 µg of protein was isolated from each sample to continue the protocol. Proteins were reduced and alkylated by the addition of 10 mM Tris(2-carboxyethyl)phosphine hydrochloride and 40 mM chloroacetamide, and incubated for 10 min at 95 °C in the dark. Phosphoric acid was added to a final concentration of 1.2% and subsequently samples were diluted sevenfold with binding buffer containing 90% methanol in 100 mM TEAB, pH 7.55. The samples were loaded on the 96-well S-Trap plate (Protifi) and a Resolvex A200 positive-pressure workstation (Tecan) was used for semi-automatic processing. After protein binding, the S-trap plate was washed three times with 200 µl binding buffer. A new deep-well plate was placed below the 96-well S-Trap plate and trypsin (1/100, w/w) was added for digestion overnight at 37 °C. Also using the Resolvex A200 workstation, peptides were eluted three times, first with 80 µl 50 mM TEAB, then with 80 µl 0.2% formic acid (FA) in water and finally with 80 µl 0.2% FA in water/acetonitrile (ACN) (50/50, v/v). Eluted peptides were dried completely by vacuum centrifugation.

TMTpro 18-plex labels (0.5 mg, Thermo Fisher Scientific) were equilibrated to room temperature immediately before use and dissolved in 20 µl anhydrous ACN. The dried peptides were resuspended in 90 µl 100 mM TEAB (pH 8.5), the peptide concentration was determined on a Lunatic spectrophotometer (Unchained Labs)[40] and the peptide amount was adjusted to 50 µg for each sample. Peptides were labelled for 1 h at room temperature using 0.25 mg of TMTPro label (labels used: 126, 127C, 128C: K14CrER Rosa SmoM2 dermis ear replicates; 127N, 128N, 129N: K14CrER Rosa SmoM2 dermis back skin replicates; 129C, 132C, 133C: wild-type dermis ear replicates; 130N, 133N, 134N: wild-type dermis back skin replicates). The reaction was quenched for 15 min at

room temperature by adding hydroxylamine to a final concentration of 0.2%. The 12 labelled samples were combined, 100 µg labelled peptides was isolated, dried by vacuum centrifugation and redissolved in 100 µl 50 mM TEAB, and 13 IUBMB mU peptide-*N*-glycosidase F (PNGaseF, made in-house) was added for deglycosylation at 37 °C overnight. Peptides were acidified with trifluoroacetic acid (TFA) to lower the pH below 3 and desalted on reversed phase (RP) C18 OMIX tips (Agilent). The tips were first washed three times with 100 µl pre-wash buffer (0.1% TFA in water/ACN (20:80, v/v)) and pre-equilibrated five times with 100 µl of wash buffer (0.1% TFA in water) before the sample was loaded on the tip. After peptide binding, the tip was washed three times with 100 µl of wash buffer and peptides were eluted twice with 100 µl elution buffer (0.1% TFA in water/ACN (40:60, v/v)). The combined elutions were transferred to high-performance liquid chromatography (HPLC) inserts and dried in a vacuum concentrator.

Vacuum-dried peptides were redissolved in 100 µl solvent A (0.1% TFA in water/ACN (98:2, v/v)) and 95 µl was injected for fractionation by RP-HPLC (Agilent series 1200) connected to a Probot fractionator (LC Packings). Peptides were first loaded in solvent A on a 4-cm pre-column (made in-house, 250 µm internal diameter (ID), 5-µm C18 beads, Dr. Maisch) for 10 min at 25 µl min^{-1} and then separated on a 15-cm analytical column (made in-house, 250 µm ID, 3 µm C18 beads, Dr. Maisch). Elution was done using a linear gradient from 100% RP-HPLC solvent A (10 mM ammonium acetate (pH 5.5) in water/ACN (98:2, v/v)) to 100% RP-HPLC solvent B (70% ACN, 10 mM ammonium acetate (pH 5.5)) for 100 min at a constant flow rate of 3 µl min^{-1}. Fractions were collected every minute between 20 min and 92 min and pooled every 24 min to generate a total of 24 samples for liquid chromatography–tandem mass spectrometry (LC–MS/MS) analysis. All 24 fractions were dried under vacuum in HPLC inserts and stored at −20 °C until further use.

Purified peptides were redissolved in 20 µl loading solvent A (0.1% TFA in water/ACN (98:2, v/v)) and the peptide concentration was determined on a Lunatic spectrophotometer (Unchained Labs). Fifteen microlitres of each sample was injected for LC–MS/MS analysis on an Ultimate 3000 RSLCnano system in-line connected to an Orbitrap Fusion Lumos mass spectrometer (Thermo Fisher Scientific). Trapping was performed at 20 µl min^{-1} for 2 min in loading solvent A on a 5 mm trapping column (Pepmap, 300 µm ID, 5-µm C18 beads, Thermo Fisher Scientific). The peptides were separated on a 110-cm µPAC column (Thermo Fisher Scientific), kept at a constant temperature of 50 °C. Peptides were eluted by a non-linear gradient starting from 2% MS solvent B (0.1% FA in ACN) reaching 26.4% MS solvent B in 45 min, 44% MS solvent B in 55 min and 56% MS solvent B in 60 min, starting at a flow rate of 600 nl min^{-1} for 5 min, and completing the run at a flow rate of 300 nl min^{-1}, followed by a 5-min wash at 56% MS solvent B and re-equilibration with MS solvent A (0.1% FA in water).

The mass spectrometer was operated in data-dependent mode, automatically switching between MS and MS/MS acquisition in Top-Speed mode. Full-scan MS spectra (375–1,500 m/z) were acquired at a resolution of 120,000 in the Orbitrap analyser after accumulation to a target AGC value of 200,000 with a maximum injection time of 50 ms. The precursor ions were filtered for charge states (2–7), dynamic exclusion (60 s; ±10 ppm window) and intensity (minimal intensity of 5E4). The precursor ions were selected in the quadrupole with an isolation window of 0.7 Da and accumulated to an AGC target of 1.2E4 or a maximum injection time of 100 ms and activated using CID fragmentation (35% NCE). The fragments were analysed in the Ion Trap Analyzer at turbo scan rate. The ten most intense MS2 fragments were selected in the quadrupole using MS3 multi-notch isolation windows of 2 m/z. An orbitrap resolution of 60,000 was used with an AGC target of 1.0×10^5 or a maximum injection time of 118 ms and activated using HCD fragmentation (65% NCE). QCloud was used to control instrument longitudinal performance during the project[41].

LC–MS/MS runs of all 12 samples were searched together using the MaxQuant algorithm (v.2.1.3.0) with mainly default search settings, including an FDR set at 1% on the peptide and protein level. Spectra were searched against the mouse protein sequences in the Swiss-Prot database (database release version of 2022_01), containing 21,986 sequences (https://www.uniprot.org/). The mass tolerance for precursor and fragment ions was set to 4.5 and 20 ppm, respectively, during the main search. Enzyme specificity was set to the C terminus of arginine and lysine, also allowing cleavage at Arg/Lys–Pro bonds with a maximum of two missed cleavages. Variable modifications were set to oxidation of methionine residues and acetylation of protein N termini, whereas carbamidomethylation of cysteine residues was set as a fixed modification. To reduce the number of spectra that suffer from co-fragmentation, the precursor ion fraction (PIF) option was set to 75%. Only proteins with at least one unique or razor peptide were retained leading to the identification of 2,849 proteins. MS2-based quantification using TMTpro labels was chosen as quantification method and a minimum ratio count of two unique peptides was required for quantification. Further data analysis was performed with an in-house R script. Reverse database hits were removed from the MaxQuant proteingroups file, corrected reporter intensities were log2 transformed & median normalized and replicate samples were grouped. Proteins with fewer than three valid values in at least one group were removed and missing values were imputed by random sampling from a normal distribution centred around each sample's detection limit (package DEP), leading to a list of 2,781 quantified proteins that was used for further data analysis. To compare protein intensities between pairs of sample groups, statistical testing for differences between group means was performed, using the package limma. Statistical significance for differential regulation was set to an FDR (Benjamini–Hochberg method) of 0.05 and $|\log2FC| = 1$ and volcano plots were generated. The z-scored protein intensities from differentially abundant hits were plotted in a heat map after non-supervised hierarchical clustering. The mass spectrometry proteomics data have been deposited to the ProteomeXchange Consortium through the PRIDE partner repository with the dataset identifiers PXD041644 and https://doi.org/10.6019/PXD041644.

Transmission electron microscopy

For transmission electron microscopy work, samples of mouse skin tissue were cut to a minimal size (1 mm × 1 mm) and fixed with 2% glutaraldehyde/2% PFA in 0.1 M cacodylate buffer, pH 7.4. Further processing was done according to standard protocols, including a number of optimized steps for skin tissue, as described previously[42]. The resulting 60-nm ultrathin sections were analysed with a Tecnai 12 BioTwin transmission electron microscope (Thermo Fisher Scientific) and representative images were taken with a 2k CCD Veleta camera (EMSIS).

Atomic force microscopy

Atomic force microscopy measurements of ECM stiffness were performed on freshly cut 16-µm-thick cryosections using the JPK Nano Wizard 2 (Bruker Nano) atomic force microscope mounted on an Olympus IX73 inverted fluorescent microscope (Olympus) and operated using the JPK SPM control software v.5. In brief, cryosections were equilibrated in PBS supplemented with protease inhibitors and measurements were performed within 20 min of thawing the samples. Silicon nitride cantilevers with 3.5-µm colloidal particles (NanoAndMore) were used for the nanoindentation experiments. For all of the indentation experiments, forces of up to 2 nN were applied, and the velocities of cantilever approach and retraction were kept constant at 2 µm per second. Before fitting the Hertz model corrected by the tip geometry to obtain Young's modulus (Poisson's ratio of 0.5), the offset was removed from the baseline, the contact point was identified and cantilever bending was subtracted from all force curves.

Dissociation of epidermal cells and flow cytometry for cell sorting

To isolate skin epidermal cells, ears were dissected, opened in two along the cartilage with forceps and incubated in 0.25% trypsin (Gibco, Thermo Fisher Scientific) in DMEM (Gibco, Thermo Fisher Scientific) overnight at 4 °C. The back skin was first shaved with electric clippers and dissected, and the hypodermis was then removed by scratching it with a scalpel. The remaining tissue (epidermis and dermis) was finally incubated in 0.25% trypsin in DMEM overnight at 4 °C by placing the dermis in contact with the solution. The day after, the epidermis was carefully separated from the dermis by using a scalpel and then incubated on a rocking plate (100 rpm) at room temperature for 5 min. Trypsin was neutralized by adding DMEM supplemented with 5% Chelex-treated fetal calf serum (CFCS), and epidermal cells were mechanically dissociated by pipetting 10 times. Samples were filtrated on a 70-µm filter then on a 40-µm filter and washed in PBS supplemented with 2% CFCS. Single cells were incubated with a biotinylated anti-CD34 primary antibody (clone RAM34; BD Biosciences; dilution 1:50) diluted in PBS supplemented with 2% CFSC, incubated for one hour on ice on a rocking plate, and protected from light. Cells were washed with PBS supplemented with 2% CFCS, incubated for 45 min on ice, on a rocking plate, with streptavidin–APC secondary antibody (BD Biosciences; 1:400), washed again and finally resuspended in a Hoechst (10 mg ml^{-1}) solution diluted at 1:4,000 in PBS supplemented with 2% CFCS. Cell sorting was performed on a BD FACS Aria II using the FACSDiva software at the ULB Flow Cytometry Platform: living epidermal cells were gated by forward scatter, side scatter and negative for Hoechst. SmoM2-mutated cells were isolated on the basis of the expression of the YFP fused to the oncogene. SmoM2–YFP expressing cells from the hair-follicle bulge were excluded by CD34–APC staining. For wild-type tissues, living IFE and infundibulum cells were sorted on the negative expression of the CD34 marker only. A total of 20,000 cells were sorted for each sample and the samples collected from 3 different mice were pooled together to obtain a total number of 60,000 cells for both tissues: ear skin and back skin.

Single-cell RNA library preparation and sequencing

Ten thousand single cells from the back skin and ear skin were loaded onto each channel of the Chromium Single Cell 3′ microfluidic chips (V2-chemistry, PN-120232, 10X Genomics) and barcoded with a 10X Chromium controller according to the manufacturer's recommendations (10X Genomics). RNA from the barcoded cells was subsequently reverse transcribed, followed by amplification, shearing 5′ adaptor and sample index attachment. The libraries were prepared using the Chromium Single Cell 3′ Library Kit (V3-chemistry, PN-120233, 10X Genomics) and sequenced on an Illumina Novaseq 6000 (paired-end 100-bp reads).

Data analysis using single-cell transcriptomics

Sequencing reads were aligned and annotated with the mm10-2020-A reference dataset as provided by 10X Genomics and demultiplexed using CellRanger (v.5.0.0) with default parameters. Further downstream analyses were carried out individually for each of the four samples (ear SMO, ear wild type, back SMO and back wild type). Quality control and downstream analysis were performed using the Seurat R package (v.4.1.0). For each sample, all of the cells passed the following criteria: showed expression of more than 2,000 and fewer than 7,000 unique genes and had less than 10% unique molecular identifier (UMI) counts belonging to mitochondrial sequences. Read counts were normalized by the NormalizeData function of Seurat, with parameter 'normalization.method = "LogNormalize" and scale.factor=10000'. A principal component analysis (PCA) for each sample was calculated using the scaled expression data of the most variable genes (identified as outliers on a mean/variability plot, implemented in the FindVariableGenes). UMAP calculation and graph-based clustering were done for each sample using the appropriate functions from Seurat (default parameters) with the respective PCA results as input. The clusters expressing sebaceous gland markers (*Scd1*, *Lpl*, *Mgst1*, *Ldhb* and *Nrp2*) and stromal cells were excluded, and dimensionality was recalculated. The final resolutions were set to 0.5 for wild-type and 0.7 for SMO samples, after testing a range from 0.3 to 0.9. Given that the obtained clustering sensitivity for a given resolution is dependent on the number of cells of that subpopulation in each respective sample, we swept over the same range of resolutions for the other samples, to ensure the presence or absence of described clusters in all samples. Different values of the resolution parameter were tested for clustering. The resolutions selected are the best to reflect the biological heterogeneity between different cell types. In addition, to verify proliferating stages, the S-phase and GS/M-phase scores were regressed out by the CellCycleScoring function, implemented in Seurat. Gene-set enrichment analysis on individual datasets was performed using the AUCell R package, with default parameters. The gene sets for identifying cells with active gene sets are defined as EHFP signature in a previous study[28]. For visualization of the AUC score calculated by AUCell, the AUC score matrix was embedded into each dataset as an additional assay with the CreateAssayObject function of Seurat.

Mouse treatments

Mice were administered 250 µl per cm^2 of collagenase type I (Sigma; 0.5 mg ml^{-1} diluted in PBS) twice a week by subcutaneous injections in the back skin, starting two weeks after oncogene induction by tamoxifen administration. Bleomycin sulfate (Abcam, 5 mg ml^{-1} diluted in PBS) was administered twice a week by subcutaneous injections in the back skin (150–200 µl per cm^2) and in the dermis of the ear (30 µl), starting one month before oncogene induction and until six weeks after. Imiquimod (Aldara) was directly applied on the back skin five days per week, starting two weeks after oncogene induction by tamoxifen administration. To irradiate the back skin, we used a UV-LED lamp (Uwave) emitting at a wavelength of 365 nm (UVA). Mice were anaesthetized with isoflurane and then irradiated for 4 min at a distance of 20–25 cm five days per week starting one month before oncogene induction until six weeks after (ten weeks in total).

Statistical analysis and reproducibility

All statistical analyses were performed using GraphPad Prism v.7.00 and R (v.4.2.0). Data are expressed as mean ± s.e.m. Normality was tested using the Shapiro–Wilk test. For the datasets that followed normality, *P* values were estimated with a paired-end *t*-test. If the dataset followed normality and the number of observations was more than 30, a two-tailed *z*-test was used. For the datasets that did not follow normality, *P* values was calculated with the Mann–Whitney test. If there were more than three samples given as input, the Kruskal–Wallis test was used. The *P* values calculated with different tests were corrected with the Benjamini–Hochberg procedure. For all of the figures, the number of mice, the number of clones and the number of areas analysed are indicated in the figure legend. For all of the figures, the number of mice, the number of clones and the number of areas analysed are indicated in the figure legend. For all of the images, each experiment was repeated independently with similar results at least three times.

Reporting summary

Further information on research design is available in the Nature Portfolio Reporting Summary linked to this article.

Data availability

All of the raw sequencing data have been deposited in the Gene Expression Omnibus (GEO) with the accession number GSE228047. All of the proteomics data have been deposited to the ProteomeXchange with the

dataset identifier PXD041644 and https://doi.org/10.6019/PXD041644. Source data are provided with this paper.

38. Pineda, C. M. et al. Intravital imaging of hair follicle regeneration in the mouse. *Nat. Protoc.* **10**, 1116–1130 (2015).
39. Aragona, M. et al. Mechanisms of stretch-mediated skin expansion at single-cell resolution. *Nature* **584**, 268–273 (2020).
40. Maia, T. M. et al. Simple peptide quantification approach for MS-based proteomics quality control. *ACS Omega* **5**, 6754–6762 (2020).
41. Chiva, C. et al. QCloud: a cloud-based quality control system for mass spectrometry-based proteomics laboratories. *PLoS ONE* **13**, e0189209 (2018).
42. Mildner, K. et al. Landmark-based retrieval of inflamed skin vessels enabled by 3D correlative intravital light and volume electron microscopy. *Histochem. Cell Biol.* **158**, 127–136 (2022).

Acknowledgements We thank the ULB animal facility and genomics core facility (F. Libert and A. Lefort); DIAPath–CMMI, which is supported by the European Regional Development Fund and the Walloon Region; E. Zindy for help and expertise in immunohistochemistry analyses; K. Midner for help with sample preparation for electron microscopy; V. Greco, P. Friedl and P. Rompolas for help and advice on the intravital imaging; and C. Dubois for her help with FACS sorting. N.B. is supported by the FRIA. P.V. is supported by the TELEVIE. The Department of Pathology at Erasme Hospital acknowledges support from 'Fonds Yvonne Boël' and 'Fonds Erasme pour la recherche médicale' (Convention d'Excellence de Gaiffier d'Emeville 2015–2021). S.A.W. was supported by the Max Planck Society and the Sigrid Juselius Foundation; Y.A.M. is the recipient of Human Frontier Science Program fellowship LT000861/2018; and C.B. is supported by the WEL Research Institute, FNRS, TELEVIE, Fond Erasme, Fondation Contre le Cancer, ULB Foundation, Fondation Julie et Francoise Drion, EOS FNRS/FWO and European Research Council.

Author contributions N.B. and C.B. designed the experiments and performed data analysis. N.B. performed most of the biological experiments. P.V. and N.B. initiated the project. R.S. performed experiments and analyses of proliferation, cell density, symmetric renewal, differentiation and apoptosis. Y.S. and A.S. performed bioinformatic analysis. D.Z., Y.A.M. and S.A.W. performed stiffness and electron microscopy experiments. I.S. and E.M. performed vital coloration and microscopic analysis. J.A. and A.C. performed immunostaining for collagen I. E.T., D.V.H. and F.I. performed proteomic analysis. N.B., R.S., P.V., A.-L.D. and M.L. performed genotyping, immunostaining and follow-ups of the mice. N.B. and C.B. wrote the manuscript. All authors read and approved the final manuscript.

Competing interests The authors declare no competing interests.

Additional information

Supplementary information The online version contains supplementary material available at https://doi.org/10.1038/s41586-023-06740-y.

Correspondence and requests for materials should be addressed to Cédric Blanpain.

Peer review information *Nature* thanks the anonymous reviewers for their contribution to the peer review of this work. Peer reviewer reports are available.

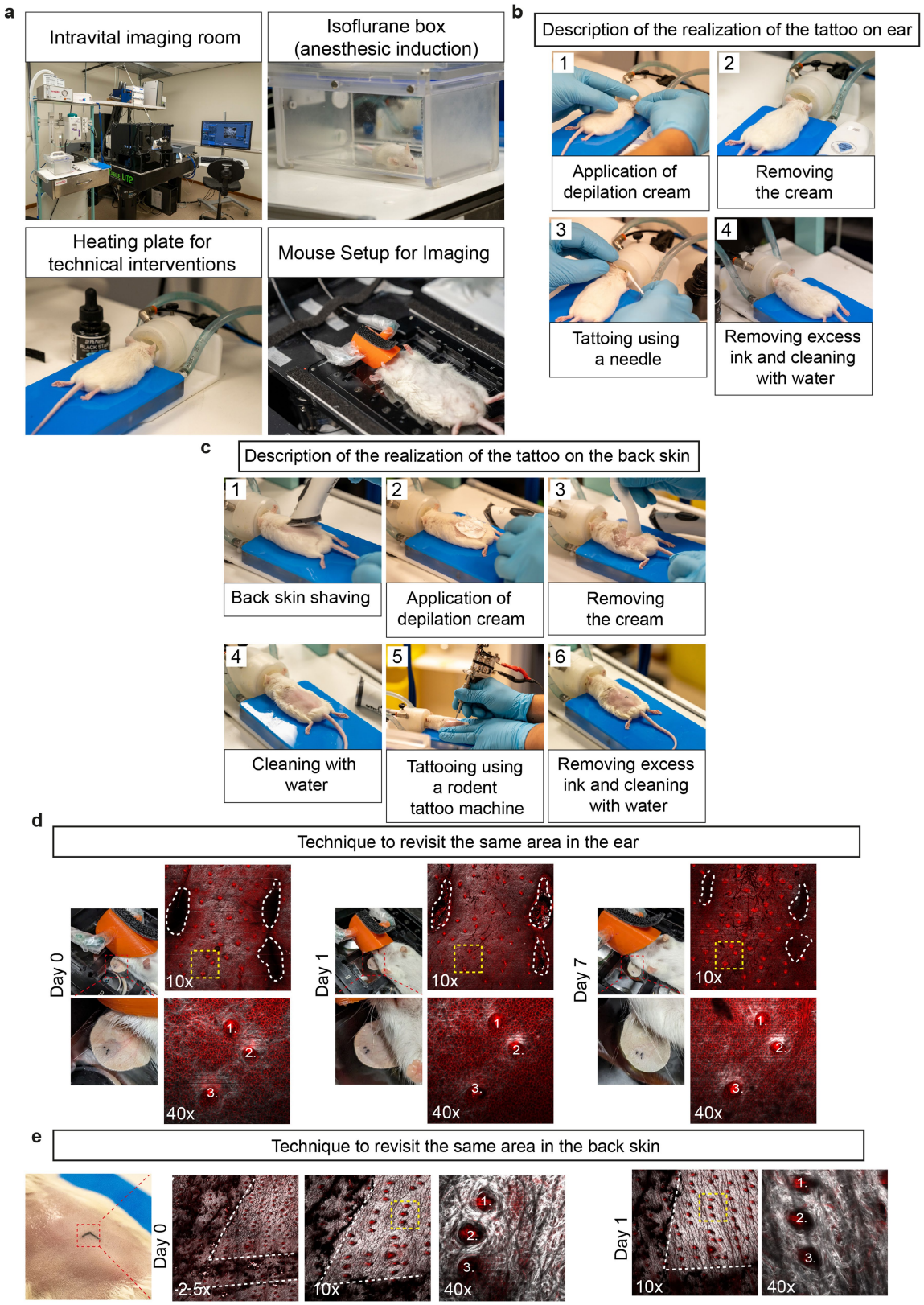

Extended Data Fig. 1 | Intravital microscopy set-up to follow the same clone over time in living mice. a, Set-up of intravital microscope. **b**,**c**, Making tattoos in the mouse ear (**b**) and back skin (**c**). **d**, Method combining tattoo and the stable pattern of hair follicles to establish spatial coordinate to monitor and track the same clones in the skin by intravital microscopy over time. For the ear, we used a 30g needle to make three punctiform tattoos. The tattoos are visible at 10× magnification. At 10× magnification, we can select an easily identifiable area using the hair follicles (yellow dashed square). At 40× magnification, we can image an area at the single-cell resolution. This area will be revisited over time to monitor cell dynamics. **e**, The same strategy is used to follow the same clones over time in the back skin, with the difference that tattooing (white dashed line) is performed using a tattoo machine. For more details, see Methods. White dashed line: delimitation of the tattoo. Hair follicles are numbered.

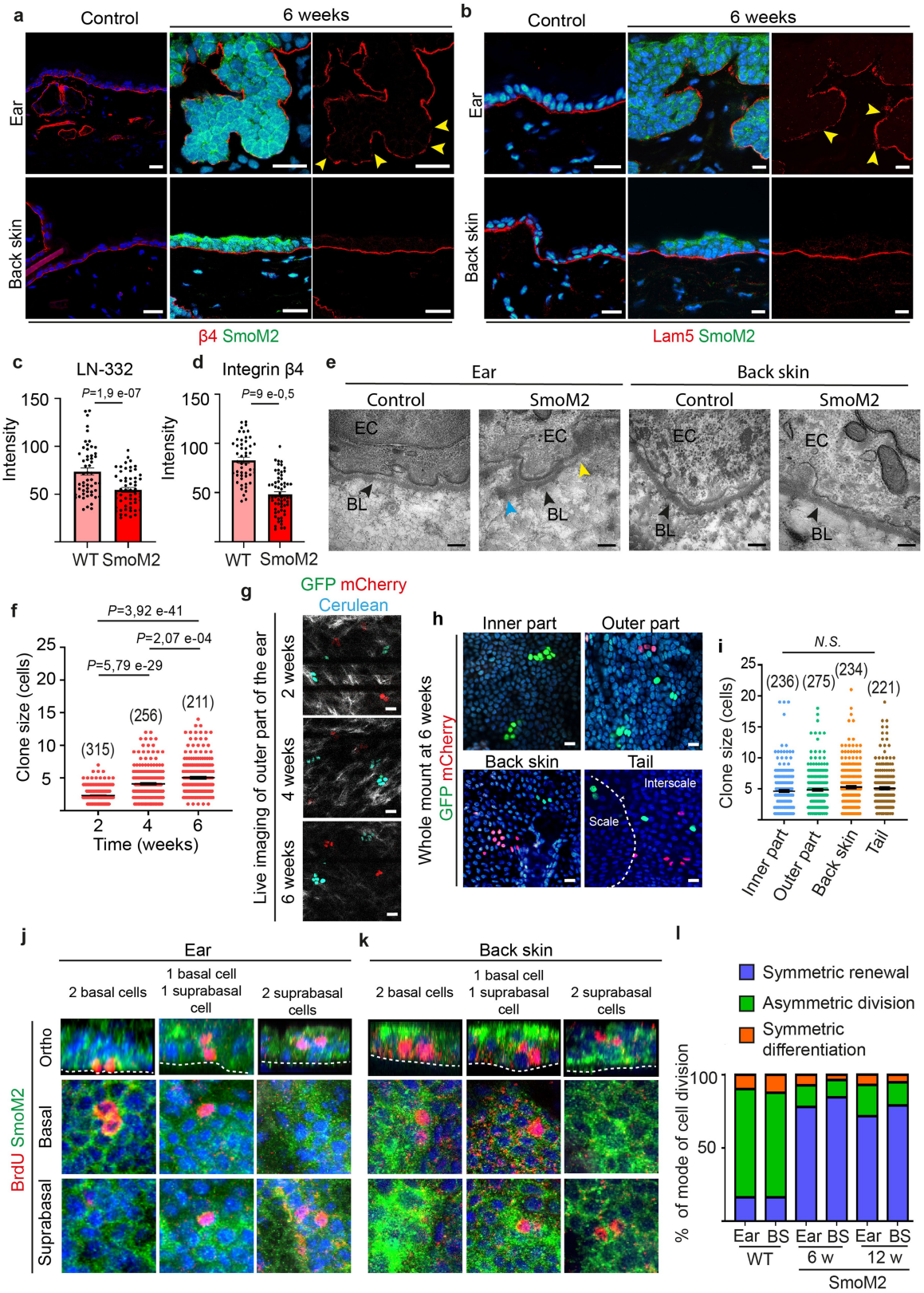

Extended Data Fig. 2 | See next page for caption.

Extended Data Fig. 2 | Clonal dynamics of normal epidermis and mode of cell division of SmoM2 cells in the ear and in the back skin. a,**b**, Microscopy analysis of β4 integrin (β4) (**a**) and Laminin-332 (Lam5) (**b**) in SmoM2 clones in the ear and the back skin 6 weeks following tamoxifen administration. Note the small disruption of the basal lamina (BL) at the leading edge of SmoM2 clones invading the dermis (yellow arrows). **c**, Quantification of the fluorescence intensity of the immunostainings of Lam5 in control and K14Cre^{ER}/Rosa-SmoM2-YFP mice 6 weeks after SmoM2 expression. Measurements were performed along the BL in control and at the leading edge of invading BCC using ImageJ. For the control, 20 areas Lam5 were analysed (n = 3). For SmoM2, 56 BCC for Lam5 (n = 3). Two-tailed z-test. **d**, Quantification of the fluorescence intensity of the immunostainings of β4 in control and K14CreER/Rosa-SmoM2-YFP mice 6 weeks after SmoM2 expression. Measurements were performed along the BL in control and at the leading edge of invading BCC using ImageJ. For the control, 21 areas for β4 were analysed (n = 3). For SmoM2, 41 BCC for β4 (n = 3). Two-tailed z-test. **e**, Transmission electron microscopical images of ear and back skin ultrathin sections from control and K14Cre^{ER}/Rosa-SmoM2-YFP mice 6 weeks after SmoM2 expression. Representative images show the remodelling of the BL (increased (blue arrow) or reduced (yellow arrow)) observed at the leading edge of BCC in the ear epidermis whereas the BL remains intact in the back skin after SmoM2 expression. EC: epidermal cell. BL: basal lamina. Scale bar: 200 nm. **f**, Quantification of the total number of cells per clone in WT ear epidermis at 2, 4, and 6 weeks after clonal marking following tamoxifen injection by intravital microscopy (n = 4). Kruskal–Wallis test. **g**, Intravital imaging of the same clones in the outer part of the ear skin at 2, 4, and 6 weeks after tamoxifen administration to K14CreER/Ichr-Ctrl-mosaic mice. **h**, Whole-mount images of epidermis of K14Cre^{ER}/Ichr-Ctrl-mosaic mice from the inner and outer part of the ear, the back and the tail at 45 days after tamoxifen administration. 40x Magnification. **i**, Quantification of the number of cells per clones at 6 weeks on whole mount of epidermis of K14Cre^{ER}/Ichr-Ctrl-mosaic. The number of basal cells found by intravital microscopy was similar to the one found by whole-mount immunostaining. (n = 4 mice). Kruskal–Wallis test. **j**,**k**, BrdU pulse-chase analysis to analyse the fate of two dividing daughter cells (doublets). Whole-mount images of SmoM2 clones in the ear (**j**) and the back skin (**k**) showing the location of BrdU doublets: two BrdU+ basal cells, one basal and one suprabasal BrdU+ cells or two suprabasal BrdU+ cells. **l**, Percentage of cell-fate outcome in WT and SmoM2 cells in the ear and in the back skin. WT ear cells (61 BrdU+ doublets from 3 mice), ear 6 weeks SmoM2 clones (110 BrdU+ doublets from 4 mice), ear 12 weeks SmoM2- clones (85 BrdU+ doublets from 3 mice), WT back skin cells (113 BrdU+ doublets from 3 mice), 6 weeks SmoM2 clones (137 BrdU+ doublets from 4 mice) and 12 weeks SmoM2 clones (115 BrdU+ doublets from 3 mice). These data show that in WT ear and back skin, most division present asymmetric cell-fate outcome, whereas most SmoM2 cells in WT ear and back skin divide symmetrically. **a**,**b**,**g**,**h**, Scale bars, 20 µm. **f**,**i**, In parentheses, the number of clones. **c**,**d**,**f**,**i**, Mean ± s.e.m.

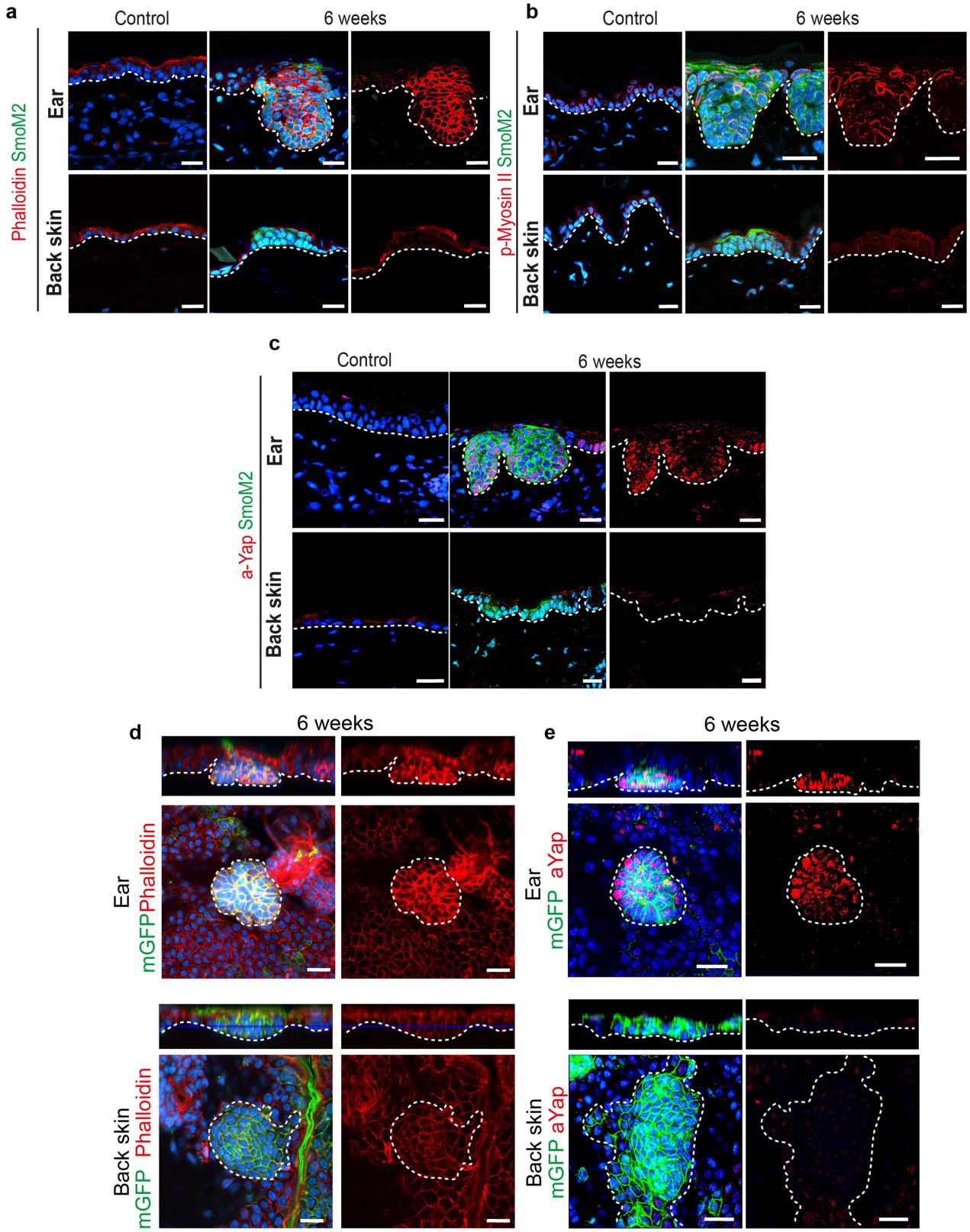

Extended Data Fig. 3 | See next page for caption.

Extended Data Fig. 3 | Expression of actin, phospho-myosin and active YAP in SmoM2 clones in the ear and in the back-skin epidermis. **a**,**b**, Immunostainings for actin (phalloidin) (**a**) and phospho-myosin II (P-Myosin II) (**b**) in control and K14Cre^{ER}/Rosa-SmoM2-YFP mice at 6 weeks after SmoM2 expression, revealing an increase in the level of F-actin (a) and phospho-myosin II (b) in SmoM2 cells in the ear. In addition, some WT cells at the border of the ear clones were also positive for phospho-myosin II. No change of phalloidin or phospho-myosin II was found in the back skin. Red: Phalloidin or phospho-myosin II; Blue: Hoechst. Scale bars, 20 µm. **c**, Immunostainings for active Yap (aYap) in control and K14Cre^{ER}/Rosa-SmoM2-YFP mice at 6 weeks after SmoM2 activation, revealing an increase expression of nuclear YAP at the leading edge of SmoM2-expressing clones and in the WT cells at the border of the clone in the ear. Only rare nuclear YAP expressing cells were found in the SmoM2-expressing cells of the back skin. Red: aYAP (d) Green: SmoM2; Blue: Hoechst. Scale bars, 20 µm. **d**,**e**, Immunostainings on whole mount for actin (phalloidin) (**d**) and active Yap (aYap) (**e**) in K14Cre^{ER}/Rosa-SmoM2-YFP/Rosa-mT/mG 3 weeks after SmoM2 activation, showing a higher level of actin expression and aYap in SmoM2 cells in the ear. No change of actin or aYap was found in the back skin. Blue: Hoechst. Scale bars, 20 µm.

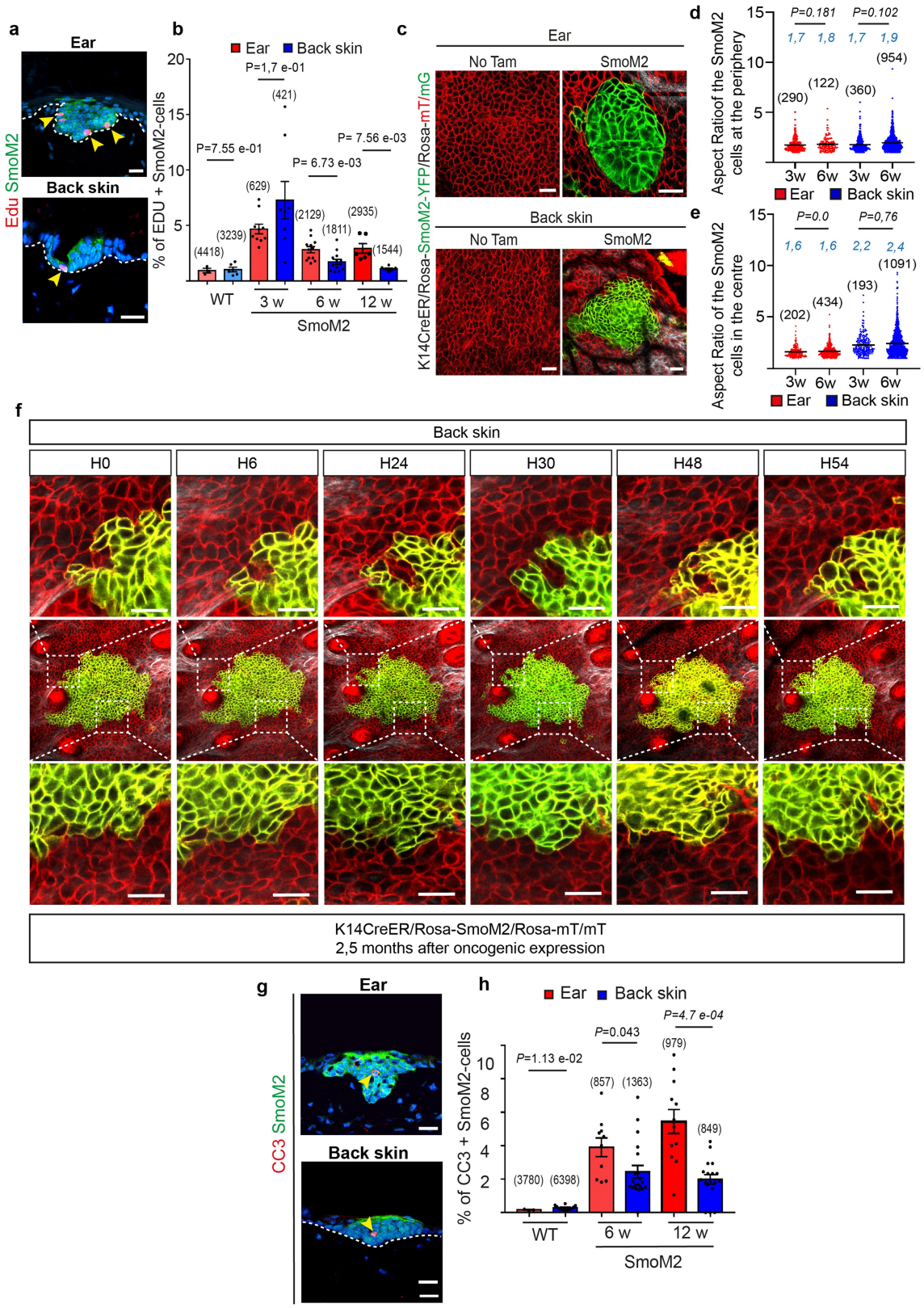

Extended Data Fig. 4 | See next page for caption.

Extended Data Fig. 4 | Cell competition, proliferation and apoptosis surrounding SmoM2 clones in the back skin and in the ear.
a, Immunostainings of EdU in the ear and the back skin of K14Cre^{ER}/Rosa-SmoM2-YFP 6 weeks after SmoM2 expression. **b**, Quantification EdU-positive cells in SmoM2 clones in K14Cre^{ER}/Rosa-SmoM2-YFP at 3 (n = 3), 6 (n = 4 for the ear and n = 5 for the back skin), and 12 weeks (n = 3) after SmoM2 activation showing an increase of proliferation in SmoM2 clones compared to the control (n = 3). Mean ± s.e.m. *t*-test. **c**, Intravital microscopy analysis of the cell density in WT cells and SmoM2 clones in the ear and the back skin of K14Cre^{ER}/Rosa-mT/mG and K14Cre^{ER}/Rosa-SmoM2-YFP/Rosa-mT/mG before and at 6 weeks after SmoM2 expression. **d**,**e**, Quantification of aspect ratio of the SmoM2 cells at the border (**d**) and at the centre (**e**) of the clone 3 and 6 weeks after SmoM2 expression. These data show that the SmoM2 cells adopt an elongated shape in the ear whereas in the back skin, SmoM2 cells are more deformed in the centre of the clones than at the periphery. In blue, the average. n = 3 mice for each conditions. Mean ± s.e.m. Two-tailed z-test. **f**, Time-lapse intravital microscopy analysis of a SmoM2-clone in the back skin of K14Cre^{ER}/Rosa-SmoM2-YFP/Rosa-mT/mG mouse 10 weeks after tamoxifen administration at different time points for 56 h showing the clonal expansion of SmoM2 cells and out competition of WT cells surrounding the SmoM2-clone. **g**, Immunostaining of cleaved Caspase 3 (CC3) in ear and the back skin of K14Cre^{ER}/Rosa-SmoM2-YFP at 6 weeks after oncogenic expression. Scale bar, 20 µm. **h**, Quantification of CC3+ cells in WT cells and SmoM2 −clones at 3, 6, and 12 weeks after SmoM2 activation showing the increase of apoptosis in SmoM2 clones. Mean ± s.e.m. *t*-test. **a**,**c**,**f g**, Scale bars, 20 µm. **b**,**d**,**e**,**h**, In parentheses, the number of cells.

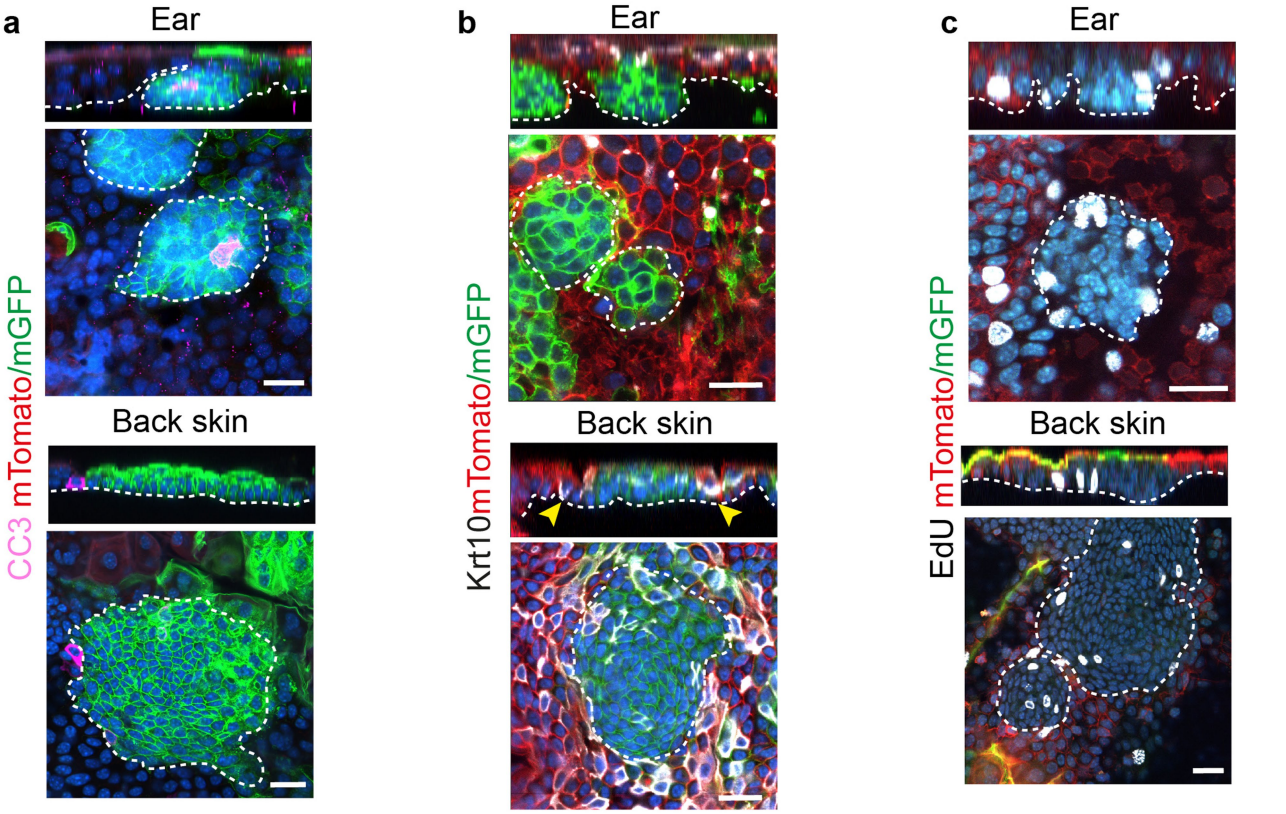

Extended Data Fig. 5 | Cell competition, proliferation and apoptosis surrounding SmoM2 clones in the back skin and in the ear by whole-mount imaging. a–**c**, Immunostaining on whole-mount back skin and ear epidermis for cleaved caspase 3 (CC3) (**a**), keratin 10 (Krt10) (**b**) and EdU (**c**) in K14Cre^{ER}/Rosa-SmoM2-YFP/Rosa-mT/mG 6 weeks after SmoM2 activation. These data show WT apoptotic cells and basal cells expressing K10 at the edge of the SmoM2-clone in the back skin and not in the ear. In the ear and the back skin, Edu-positive cells are more present at the periphery of the clone. Scale bars, 20 µm.

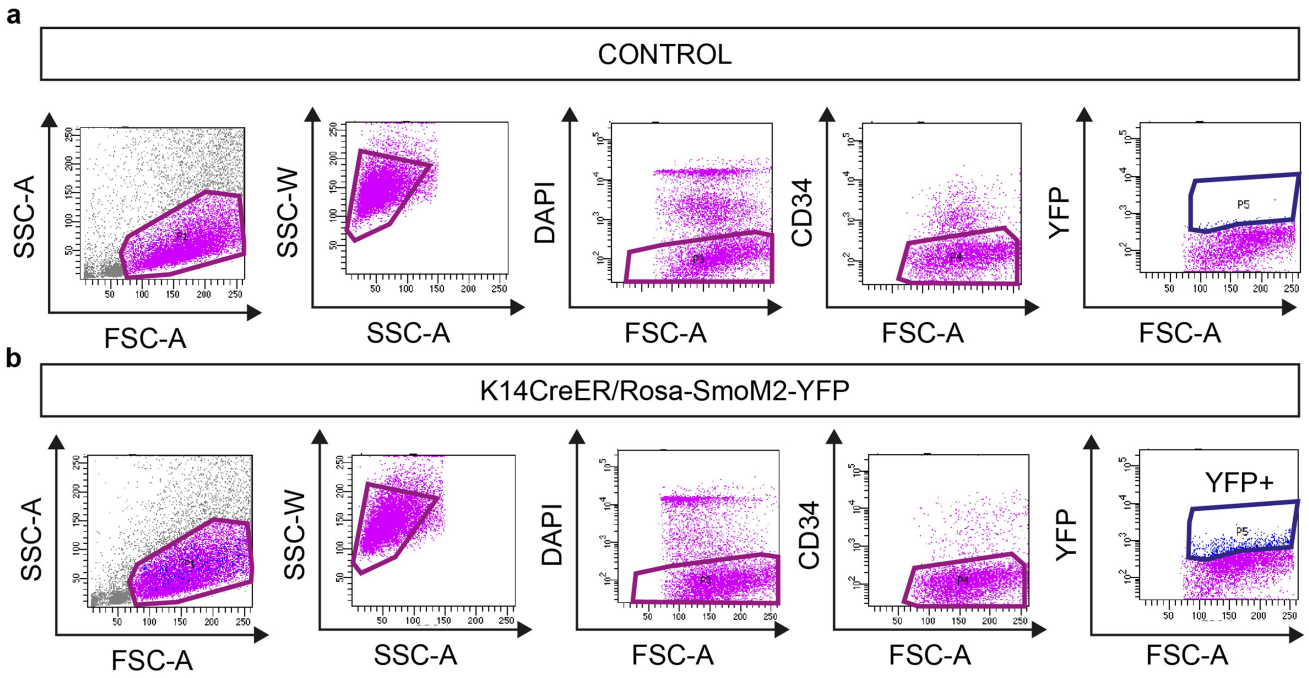

c

CLUSTERS	CLUSTER SPECIFIC GENES
SC/CP G0 I	Ccnd2, Fth1, Sostdc1, Krt15
SC/CP G0 II	Krt14, Mt1, Krt5, Sparc
SC/CP G0 III	Igfbp3, Igfbp2, Igfbp7 Wnt4, , ,
SC/CP G1S	Mcm2, Mcm3, Mcm6, Mcm5, Lig1, Mcm7, E2f1
SC/CP G2M	Cdk1, Aurkb, Birc5, Ccna2, Cenpf
IFE Diff	Krt1, Krt10, Sbsn, Klf4, Ly6g6c, Mt4
Committed	Krt5, Krtdap, Ly6d, Gata3, Hes1, Mt2
SG	Scd1, Lnc2, Lpl, Mgst1,
INF Prog	Foxc1, Lrig1, Plet1, Lgr6, Sox9, Aldh3a1
INF Diff	Gata6, Krt79, Defb6, Defb1, Ly6g6c
Early EHFP	Lhx2, Gli1, Lgr5
EHFP	Lhx2, Lgr5, Sox9, Mycn
HH responsive	Ptch1, Gli1

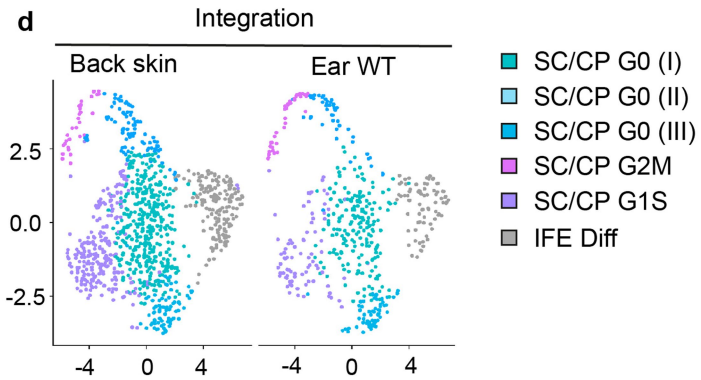

Extended Data Fig. 6 | Single-cell RNA-seq analysis of WT cells and SmoM2 epidermal cells, and FACS sorting strategy. a,**b**. Fluorescence activated cell sorting (FACS) plots showing the gating strategy used to FACS isolate the proportion of SmoM2-YFP in control mice (**a**) and K14Cre^{ER}/Rosa-SmoM2-YFP mice (**b**) 6 weeks after oncogenic expression. **c**, Table showing the genes used to annotate the different clusters. **d**, UMAP graphic of the clustering analysis for single-cell RNA-seq of the WT ear and back-skin epidermis after data integration using Seurat.

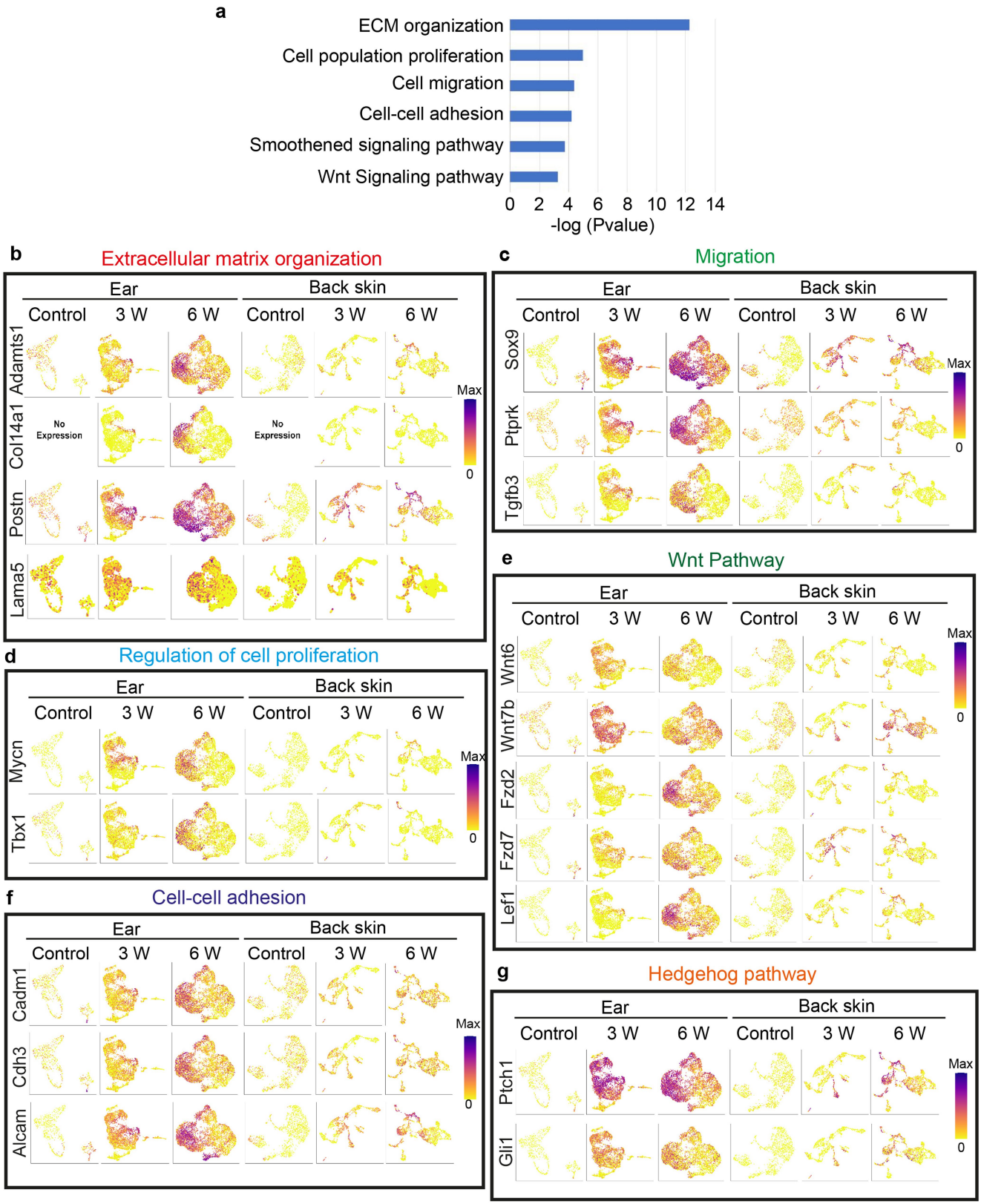

Extended Data Fig. 7 | Gene ontology of EHFP-associated genes. a, Gene ontology analysis of the genes upregulated in the ear 6 W EHFP cluster. Statistics are based on the permutation method. **b**–**g**, UMAP plot of the ear and back samples coloured by the level of normalized gene expression values for genes regulating ECM organization or basal lamina (**b**), migration (**c**), cell proliferation (**d**), the WNT pathway (**e**), cell–cell adhesion (**f**) or the Hedgehog pathway (**g**).

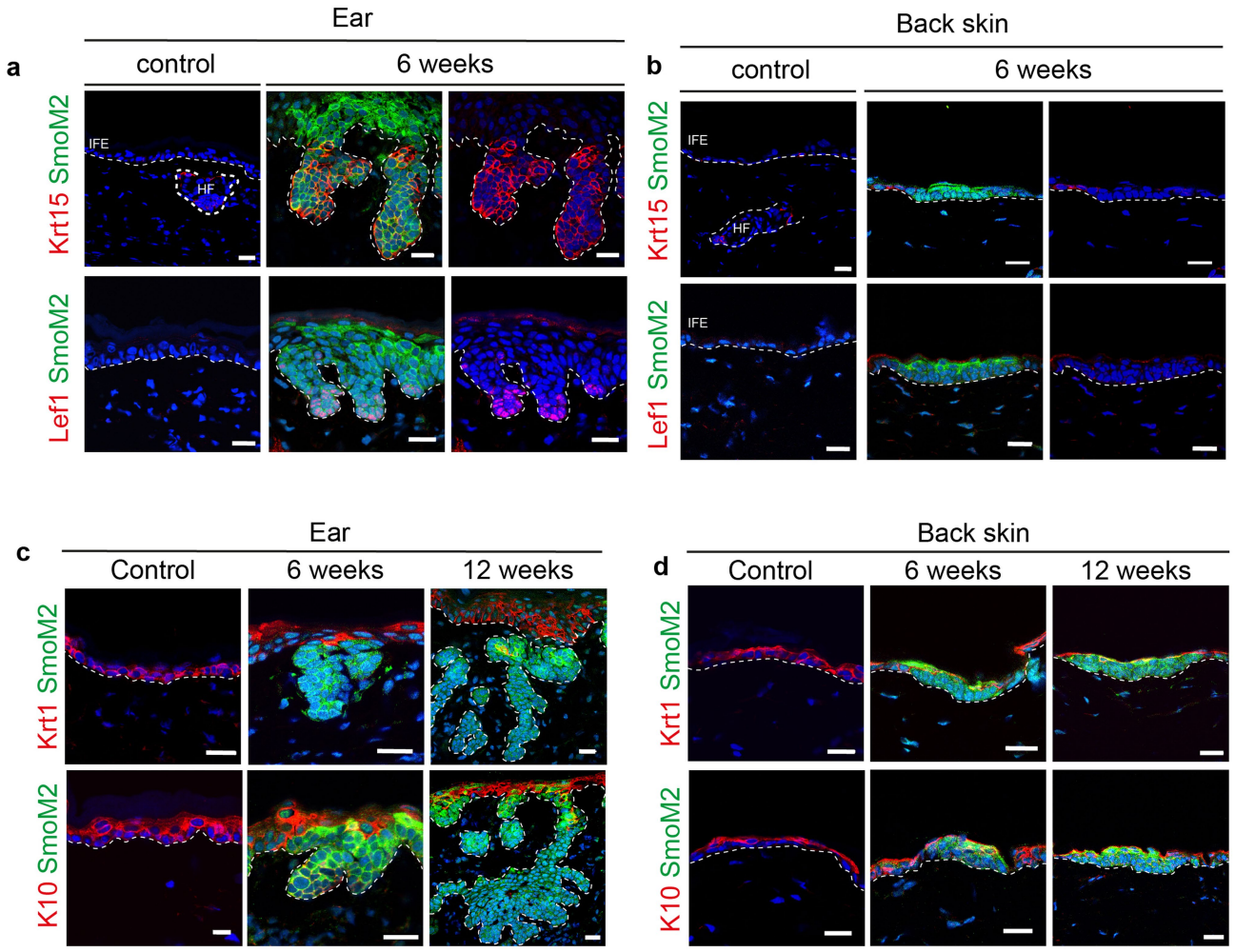

Extended Data Fig. 8 | EHFP reprogramming and block of normal IFE differentiation in SmoM2-expressing cells in the ear but not in the back-skin epidermis. a,**b**, Immunostaining of ear skin (**a**) and back skin (**b**) for K15, LEF1 and SmoM2–YFP in control and in K14Cre^{ER}/Rosa-SmoM2 mice at 6 and 12 weeks after tamoxifen induction. SmoM2 cells in the ear skin are reprogrammed into EHFP-like cells. **c**,**d**, Immunostaining of ear skin (**c**) and back skin (**d**) for K1, K10 and SmoM2–YFP in control and in K14Cre^{ER}/Rosa-SmoM2-YFP mice at 6 and 12 weeks after tamoxifen induction. SmoM2 cells in the back skin differentiate into K1/K10-positive cells. These immunostaining analyses also confirmed the expression of normal differentiation marker K1 in the suprabasal cells of the SmoM2-expressing cells in the back skin and the repression of the differentiation in SmoM2-expressing clones in the ear epidermis. IFE, interfollicular epidermis; HF, hair follicle. **a**–**d**, Scale bars, 20 μm.

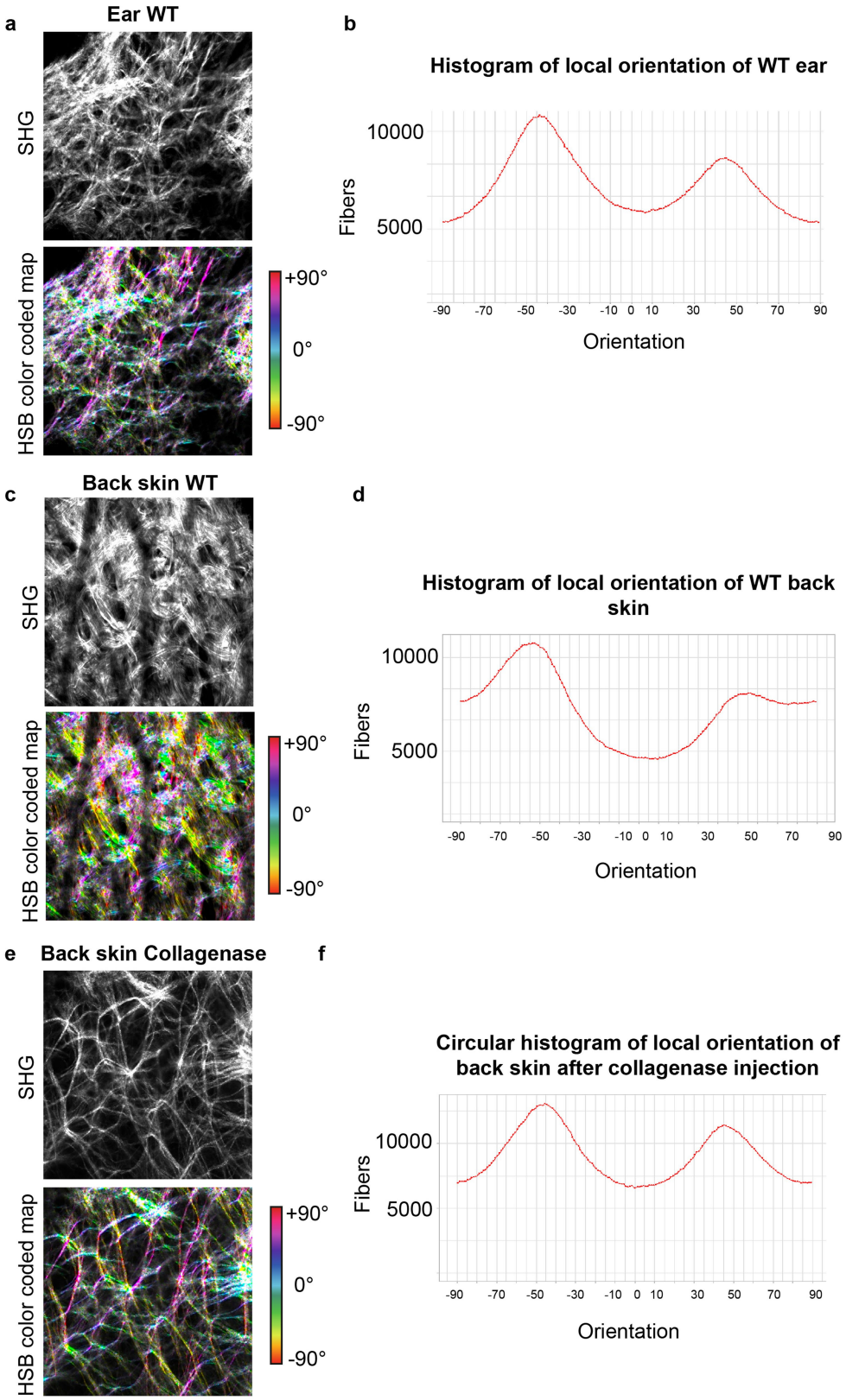

Extended Data Fig. 9 | Orientation of collagen-fibre bundles in the ear and in the back skin. a–**f**, Angular distribution of collagen-fibre bundles measured by OrientationJ software from SHG images of the dermis of the WT ear (**a**,**b**) and the back skin before (**c**,**d**) and after (**e**,**f**) collagenase administration. HBS colour-coded map (**a**,**c**,**e**) and histogram of local angles (**b**,**d**,**f**) showing the orientation of collagen-fibre bundles. The orientation of the collagen bundles was relatively similar in the two locations.

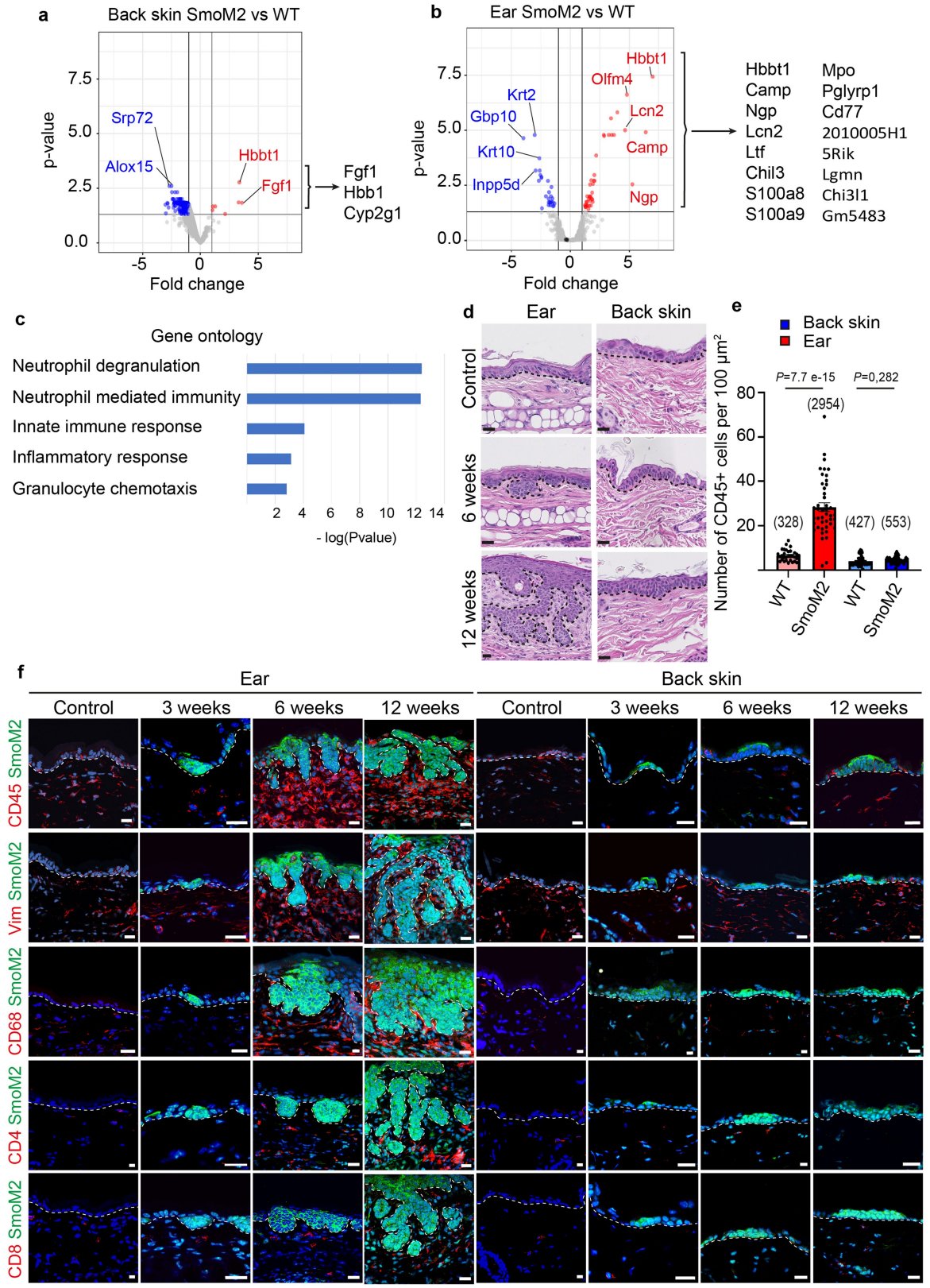

Extended Data Fig. 10 | See next page for caption.

Extended Data Fig. 10 | ECM composition and remodelling in the ear and in the back skin after SmoM2 expression. a,**b**, Quantitative proteomic analysis of the dermis after SmoM2 expression in the ear (**a**) and the back skin (**b**). Volcano plot indicating the differentially expressed proteins. Proteins upregulated in SmoM2 dermis (red dot) or in WT dermis (blue dot). A total of 742 proteins were significantly downregulated, and 7 proteins were significantly upregulated in SmoM2 back-skin dermis samples. Proteomic analysis shows that only very few proteins were more upregulated in the dermis of back skin after SmoM2 expression. Twenty-seven proteins were significantly upregulated in WT ear dermis and 40 proteins were significantly upregulated in SmoM2 ear dermis, which contains a higher number of proteins expressed by inflammatory cells after oncogenic expression in the ear. Statistical significance for differential regulation is set at FDR < 0.05 and fold change of 2 ($|\log2FC| \geq 1$). **c**, Gene ontology analysis of the proteins upregulated in the SmoM2 ear at 6 weeks after oncogenic expression. Statistics are based on the permutation method. **d**, H&E staining in control and K14Cre^{ER}/Rosa-SmoM2-YFP mice of the ear and back skin at 1.5 and 3 months after SmoM2 activation. **e**, Quantification of CD45^{+} cells in the dermis of the ear and the back skin in WT and SmoM2 mice at 6 weeks after SmoM2 expression showing the increase of the inflammation in the dermis of the ear after SmoM2 expression but not in the back skin. For each condition, at least 10 areas (40×) per mice (n = 3) were analysed. In parentheses, number of CD45^{+} cells. Mean ± s.e.m. Paired *t*-test, with two-sample unequal variance (heteroscedastic). **f**, Immunostaining for CD45 (pan-immune cells), Vimentin (fibroblasts and inflammatory cells), CD68 (macrophages), CD4 (T helper lymphocytes), CD8 (T cytotoxic lymphocytes) and SmoM2 in control and K14Cre^{ER}/Rosa-SmoM2-YFP mice at 3, 6, and 12 weeks after SmoM2 expression, revealing a strong recruitment of immune cells in particular macrophages (CD45^{+} CD68^{+}) and fibroblasts (Vimentin^{+}) in the SmoM2-expressing cells that invade the ear dermis. No inflammatory cell infiltration is observed in the dermis of the back skin. Scale bars, 20 µm.

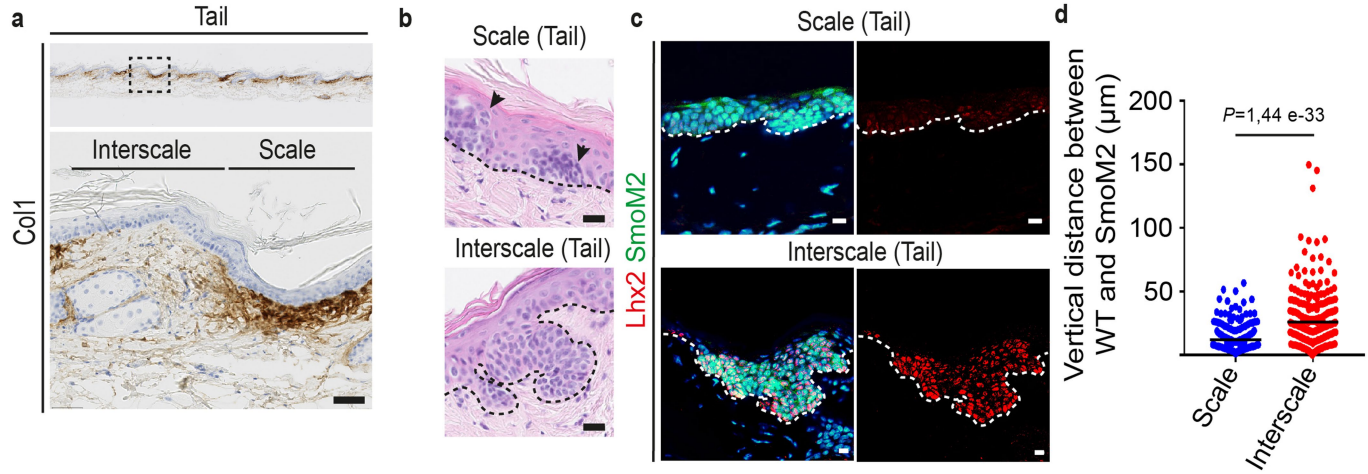

Extended Data Fig. 11 | The level of collagen I expression correlates with the competence for BCC initiation in the tail skin. a, Collagen I immunohistochemistry of the scale and interscale regions of the tail. The level of collagen I is higher in the scale compared to the interscale of the tail. Scale bar, 50 µm. **b**, H&E stainings in the tail skin of K14Cre^{ER}/Rosa-SmoM2-YFP mice at 6 weeks after SmoM2 activation, showing that BCC arises from the interscale epidermis whereas the tail scale epidermis (as the back skin) is resistant to SmoM2-induced tumorigenesis. **c**, Immunostaining of LHX2 in the tail of K14Cre^{ER}/Rosa-SmoM2-YFP mice 6 weeks after SmoM2 activation. Scale bars, 20 µm. **d**, Quantification of tumour invasion measured by the vertical distance between WT cells and SmoM2 cells in the tail dermis at 6 weeks after SmoM2 activation. SmoM2 clones in the interscale but not in the scale of the tail skin invade the dermis. A total of 366 clones in the scale region and 318 clones in the interscale region of the tail have been quantified from 3 mice. Mean ± s.e.m. Kruskal–Wallis test.

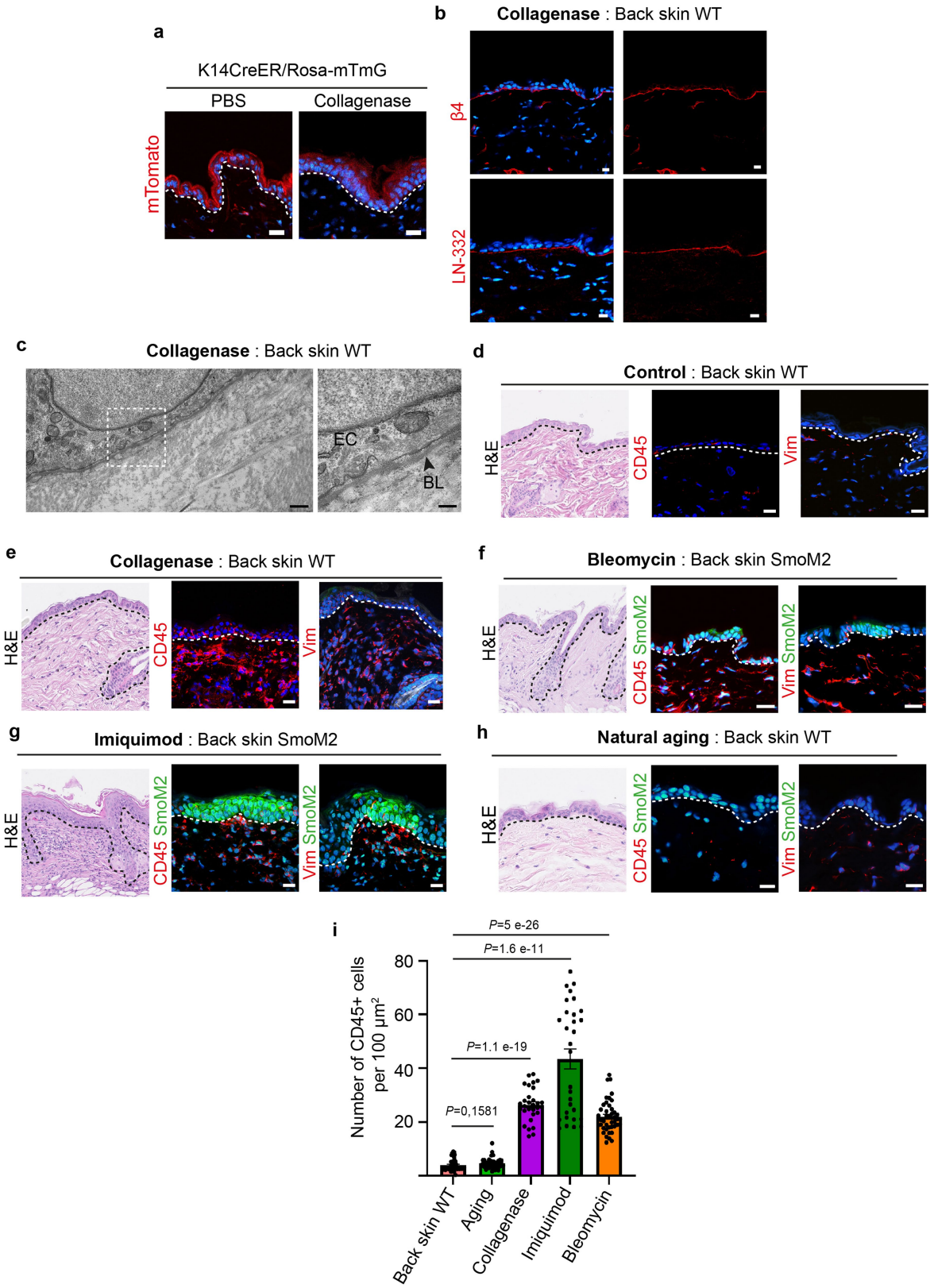

Extended Data Fig. 12 | See next page for caption.

Extended Data Fig. 12 | Inflammation in the back skin does not promote the invasion of SmoM2-expressing cells. a, Immunostaining of back skin after intradermal injection of PBS (left) or collagenase (right) in control mouse ($K14Cre^{ER}$/Rosa-mT/mG), showing the absence of dermal invasion of normal epidermis. **b**,**c**. Immunostaining for β4 and Lam5 (**b**) and electron microscopy imaging (**c**) of the back skin of WT mice (control) and after collagenase injection showing that the BL remains intact after collagenase injection. Scale bars, 20 μm. EC, epidermal cell; BL, basal lamina. Scale bars for EM images: 500 nm (left) and 200 nm (right). **d**–**h**, H&E and immunostaining for CD45 (immune cells) and vimentin (immune cells and fibroblasts) of back skin in control mice (**d**), one day after collagenase injection (**e**), of back skin of $K14Cre^{ER}$/Rosa-SmoM2-YFP mice at 6 weeks after oncogene expression following bleomycin administration for 1 month (**f**), of back skin of $K14Cre^{ER}$/Rosa-SmoM2-YFP mice at 6 weeks after oncogene expression following daily application of imiquimod for 1 month (**g**), of back skin in $K14Cre^{ER}$/Rosa-SmoM2-YFP 1.5-year-old mice at 6 weeks after oncogene expression (**h**). Scale bars, 20 μm. **i**, Quantification of $CD45^+$ cells in the dermis of the back skin in WT and SmoM2 mice in different inflammatory conditions (collagenase, imiquimod, bleomycin) and in old mice. For the control SmoM2, 472 $CD45^+$ cells for WT (n = 3). For the old mice, 569 $CD45^+$ cells from 41 area (n = 2). For imiquimod, 2,801 $CD45^+$ cells from 30 areas (n = 2). For collagenase, 2,225 $CD45^+$ cells from 30 areas (n = 2). For bleomycin, 3,094 $CD45^+$ cells from 45 areas (n = 3). These data show that inflammation induced by imiquimod and bleomycin does not promote invasion of SmoM2-expressing cells. Mean ± s.e.m. Paired *t*-test, with two-sample unequal variance.

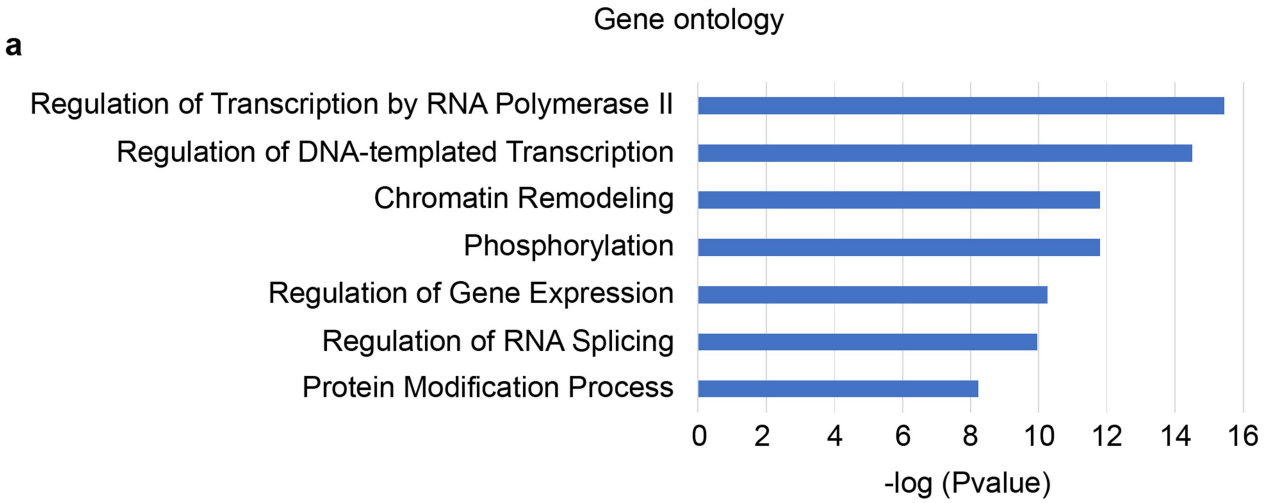

Extended Data Fig. 13 | Gene ontology of SmoM2 cells of the back skin. a, Gene ontology analysis of the genes upregulated in the all of the SmoM2 cells of the back skin 6 weeks after oncogenic expression versus the WT cells of the back skin. Statistics are based on the permutation method.

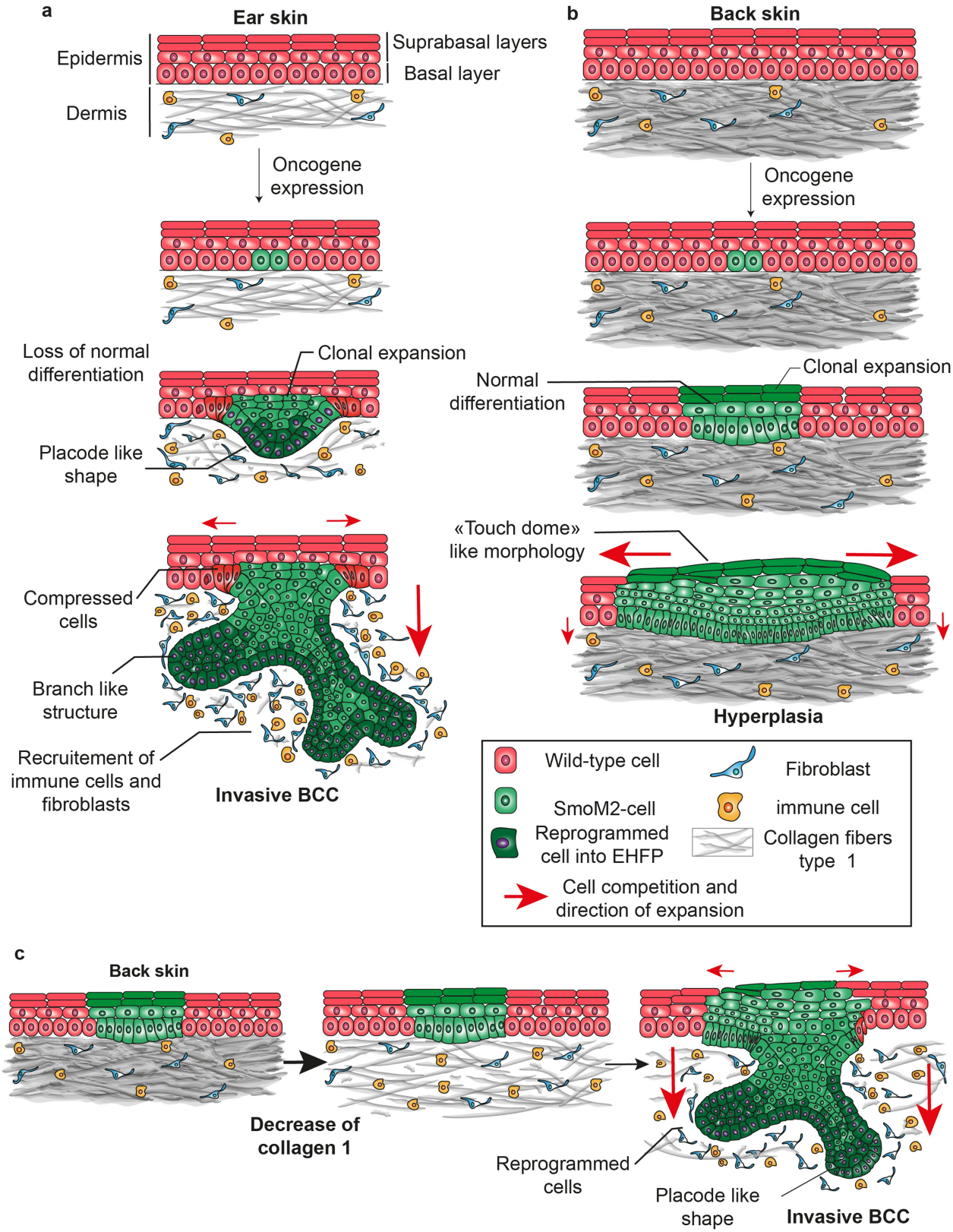

Extended Data Fig. 14 | Model summarizing how ECM composition dictates the mode of cell competition and competence for tumour initiation. **a**, Oncogenic Hedgehog activation by the SmoM2 oncogene induces BCC in the ear epidermis. SmoM2 cells adopt a placode-like shape, lose their ability to differentiate and are reprogrammed into an EHFP-like fate. The SmoM2 clones compress the WT cells at the edge. SmoM2 clones invade the dermis until they form a branch-like structure and become invasive BCCs. **b**, Oncogene-expressing cells in the back-skin epidermis undergo clonal expansion in a lateral manner without leading to tumour invasion. SmoM2 cells are very efficient at outcompeting the WT cells but lack the ability to become invasive. The high level of collagen I in the dermis of the back skin restricts BCC development and imposes a lateral clonal expansion of oncogene-expressing cells. **c**, Decreasing the abundance of collagen by collagenase injection, during natural ageing and after chronic UVA exposure overcomes the natural resistance to BCC development in the back skin.

nature portfolio

Corresponding author(s): Blanpain Cédric

Last updated by author(s): 06/09/2023

Reporting Summary

Nature Portfolio wishes to improve the reproducibility of the work that we publish. This form provides structure for consistency and transparency in reporting. For further information on Nature Portfolio policies, see our Editorial Policies and the Editorial Policy Checklist.

Statistics

For all statistical analyses, confirm that the following items are present in the figure legend, table legend, main text, or Methods section.

n/a	Confirmed
☐	☒ The exact sample size (*n*) for each experimental group/condition, given as a discrete number and unit of measurement
☐	☒ A statement on whether measurements were taken from distinct samples or whether the same sample was measured repeatedly
☐	☒ The statistical test(s) used AND whether they are one- or two-sided *Only common tests should be described solely by name; describe more complex techniques in the Methods section.*
☒	☐ A description of all covariates tested
☐	☒ A description of any assumptions or corrections, such as tests of normality and adjustment for multiple comparisons
☐	☒ A full description of the statistical parameters including central tendency (e.g. means) or other basic estimates (e.g. regression coefficient) AND variation (e.g. standard deviation) or associated estimates of uncertainty (e.g. confidence intervals)
☐	☒ For null hypothesis testing, the test statistic (e.g. *F*, *t*, *r*) with confidence intervals, effect sizes, degrees of freedom and *P* value noted *Give P values as exact values whenever suitable.*
☒	☐ For Bayesian analysis, information on the choice of priors and Markov chain Monte Carlo settings
☒	☐ For hierarchical and complex designs, identification of the appropriate level for tests and full reporting of outcomes
☒	☐ Estimates of effect sizes (e.g. Cohen's *d*, Pearson's *r*), indicating how they were calculated

Our web collection on statistics for biologists contains articles on many of the points above.

Software and code

Policy information about availability of computer code

Data collection	Zen Black or Zen Blue 3.3 (Zeiss) FACSDiva software Software 8.0.1 JPK SPM control software v.5
Data analysis	All statistical analyzes were carried out using GraphPad Prism version 7.00 and R (version 4.1.0). Data are expressed as mean ± standard bar error of the mean (S.E.M). Quantification of the depth of invasion, the clone size, the number of cells, and ration between the height and width were performed using Zen Black or Zen Blue (Zeiss Software). For immunohistochemistry, the slides were digitized using slide scanners Nanozoomer 2.0 HT (Hamamatsu, Hamamatsu City, Japan) and analyzed using QuPath (0.3.2). Measurements of the intensity of SHG, measurement of the Aspect Ratio (AR) of epidermal cells, collagen fiber bundles measurements were analyzed in ImageJ/Fiji software. For the orientation of the collagen fiber bundles, we used the plug-in OrientationJ in ImageJ to generate the HBS color code and the histogram of local angles. Atomic force microscopy (AFM) measurements of extracellular matrix stiffness were performed using the JPK SPM control software v.5 For the Single cell-RNA-seq,

10,000 single cells from the back skin and ear skin were loaded onto each channel of the Chromium Single Cell 3′ microfluidic chips (V2-chemistry, PN-120232, 10X Genomics) and barcoded with a 10X Chromium controller according to the manufacturer's recommendations (10X Genomics). The libraries were prepared using the Chromium Single Cell 3′ Library Kit (V3-chemistry, PN-120233, 10X Genomics) and sequenced on an Illumina Novaseq 6000 (paired-end 100bp reads). Sequencing reads were aligned and annotated with the mm10-2020-A reference dataset as provided by 10X Genomics and demultiplexed using CellRanger (v.5.0.0) with default parameters. Quality control and downstream analysis were performed using the Seurat R package (v.4.1.0). Read counts were normalized by NormalizeData function of Seurat, with parameter 'normalization.method = "LogNormalize" and scale.factor=10000'. A PCA for each sample was calculated using the scaled expression data of the most variable genes (identified as outliers on a mean/variability plot, implemented in the FindVariableGenes). UMAP calculation and graph-based clustering were done for each sample using the appropriate functions from Seurat (default parameters) with the respective PCA results as input. In addition, to verify proliferating stages, the S-phase and GS/M-phase scores were regressed out by CellCycleScoring function, implemented in the Seurat. Geneset enrichment analysis on individual dataset was performed using AUCell R package, with default parameters. For visualization of AUC (Area Under the Curve) score calculated by AUCell, the AUC score matrix has been embedded into each dataset as additional assay with CreateAssayObject function of Seurat.

For the LC-MS/MS analysis, runs of all 12 samples were searched together using the MaxQuant algorithm (version 2.1.3.0) with mainly default search settings, including a false discovery rate set at 1% on peptide and protein level. Proteins with less than three valid values in at least one group were removed and missing values were imputed by random sampling from a normal distribution cantered around each sample's detection limit (package DEP) leading to a list of 2,781 quantified proteins that was used for further data analysis. To compare protein intensities between pairs of sample groups, statistical testing for differences between group means was performed, using the package limma.

For manuscripts utilizing custom algorithms or software that are central to the research but not yet described in published literature, software must be made available to editors and reviewers. We strongly encourage code deposition in a community repository (e.g. GitHub). See the Nature Portfolio guidelines for submitting code & software for further information.

Data

Policy information about availability of data

All manuscripts must include a data availability statement. This statement should provide the following information, where applicable:

- Accession codes, unique identifiers, or web links for publicly available datasets
- A description of any restrictions on data availability
- For clinical datasets or third party data, please ensure that the statement adheres to our policy

Raw data of Single-cell RNA sequencing has been deposited in the Gene Expression Omnibus with the accession number GSE228047.

The mass spectrometry proteomics data have been deposited to the ProteomeXchange Consortium via the PRIDE [1] partner repository with the dataset identifier PXD041644 and 10.6019/PXD041644.

Research involving human participants, their data, or biological material

Policy information about studies with human participants or human data. See also policy information about sex, gender (identity/presentation), and sexual orientation and race, ethnicity and racism.

Reporting on sex and gender	N/A
Reporting on race, ethnicity, or other socially relevant groupings	N/A
Population characteristics	N/A
Recruitment	N/A
Ethics oversight	N/A

Note that full information on the approval of the study protocol must also be provided in the manuscript.

Field-specific reporting

Please select the one below that is the best fit for your research. If you are not sure, read the appropriate sections before making your selection.

☒ Life sciences ☐ Behavioural & social sciences ☐ Ecological, evolutionary & environmental sciences

For a reference copy of the document with all sections, see nature.com/documents/nr-reporting-summary-flat.pdf

Life sciences study design

All studies must disclose on these points even when the disclosure is negative.

Sample size	Samples size for each experiment is indicated in corresponding figure legends. The sample size was chosen based on previous experience in

Sample size	the laboratory for each experiment to yield high power to detect specific effects. The previous experiences refers to: cell at the origin of BCC, reprogramming of BCC, clonal dynamic of BCC (Youssef Nature Cell Biology 2010, Youssef Nature Cell Biology 2012, Sanchez-Danes Nature Cell Biology 2016). No statistical methods were used to predetermine sample size.
Data exclusions	No data were excluded from the analysis
Replication	All the experiments were performed in at least 3 biologically independent replicates (except for the quantification intravital back skin, for the old mice and for quantification of CD45+ cells in collagenase and Imiquimod experiments for which experiment was repeated twice. n is described in figure legends. All replicates reported in the manuscript and on which statistics are based are biological replicates. No technical replicates were used to calculate statistics. All replication attempts have been successful.
Randomization	For in vivo studies on mouse models, animals were chosen based on correct genotypes: (1) K14CREER/Rosa-SmoM2, (2) K14CREER/Rosa-SMOM2/Rosa-mTmG and (3) K14CREER/Ichr-Ctrl-mosaic. Mice were induced between 1.5 and 4 months (except for the "old mice" experiment in which the mice were old after 1.5 years). of age with Tamoxifen (Sigma-Aldrich) dissolved in 10% Ethanol and 90% sunflower oil (Sigma). The quantity of tamoxifen administrated to mice was adapted in accordance with their weight. For non-clonal induction: Mice were treated with a single intraperitoneal injection (IP) of tamoxifen at a dosage of 1mg/30g. For clonal induction : Mice were treated with a single intraperitoneal injection of tamoxifen at a dosage of 0,075mg/30g (ear skin clonal dose) or 0,4mg/30g (back skin clonal dose). For K14CREER/Ichr-Ctrl-mosaic, mice were induce with a single intraperitoneal injection of tamoxifen at a dosage of 0,5mg/30g. Mice were sacrificed at different time points post induction. For collagenase and PBS injection, 250 µl per cm2 of collagenase type I (Sigma; 0,5 mg/ml diluted in DPBS) or PBS was administrated every twice a week days by subcutaneous injections on the back skin, starting 2 weeks after oncogene induction (Tamoxifen administration). Bleomycin sulfate (Abcam, 5 mg/mL diluted in PBS) was administrated every twice a week by subcutaneous injections on the back skin (150-200 µl per cm2) and in the dermis of the ear (30 µl), starting 1 month before oncogene induction and until 6 weeks after. Imiquimod (Aldara®) was directly applied on the back skin 5 days per week, starting 2 weeks after oncogene induction (Tamoxifen administration). To irradiate the back skin, we used a UV-LED lamp (Uwave) emitting at a wavelength of 365 nm (UV-A). Mice were anesthetized with isoflurane and then irradiated for 4 min at a distance of 20-25 cm 5 days per week starting 1 month before oncogene induction until 6 weeks after (10 weeks in total). For proliferation experiments, mice were injected with a single intraperitoneal injection of EdU (2.5 mg/ml in PBS) 4hrs before sacrifice. For cell fate division, mice were injected with a single intraperitoneal injection of BrdU (1.25 µg/µl) 24hrs before sacrifice to capture the doublets of BrdU.
Blinding	Investigators were blinded to mouse and cell line genotypes or treatment conditions during experiments, for performing sample analysis, imaging and quantification.

Reporting for specific materials, systems and methods

We require information from authors about some types of materials, experimental systems and methods used in many studies. Here, indicate whether each material, system or method listed is relevant to your study. If you are not sure if a list item applies to your research, read the appropriate section before selecting a response.

Materials & experimental systems

n/a	Involved in the study
☐	☒ Antibodies
☒	☐ Eukaryotic cell lines
☒	☐ Palaeontology and archaeology
☐	☒ Animals and other organisms
☒	☐ Clinical data
☒	☐ Dual use research of concern
☒	☐ Plants

Methods

n/a	Involved in the study
☒	☐ ChIP-seq
☐	☒ Flow cytometry
☒	☐ MRI-based neuroimaging

Antibodies

Antibodies used

For FACS analysis and sorting the following antibodies were used:
anti-CD34 (rat, RAM34, BD Biosciences; dilution 1:50) and streptavidin-APC secondary antibody (BD Biosciences; 1:400)
Hoechst (10mg/ml) solution diluted at 1:4000 in PBS-2% CFCS

The following primary antibodies were used: anti-GFP (goat polyclonal; Abcam, ab6673; 1:1000), anti-GFP (rabbit polyclonal; Abcam, ab6556; 1:2000), anti-CD104/ß4 integrin (rat; BD Biosciences, 346-11A; 1:200); anti-K10 (rabbit; Covance, 905404 ; 1:2000); anti-K1 (rabbit, Covance; 1/4000), anti-K15 (chicken; Covance, 833904 ; 1/15000); anti-Lhx2 (Goat,; Santa Cruz, sc-19344; 1/500); anti-Lef1 (rabbit, cell signalling, 2230 ; 1/200); anti-P-Cadherin (Rat; Invitrogen, 32000Z ; 1/1000); anti-Vimentin (Rabbit; Abcam, 92547 ; 1/1000); anti-CD45;(Rat; BD Biosciences, 103106 ; 1/50), anti-CD68 (Rabbit; Abcam, ab125212; 1/1000) , anti-CD8 (Rabbit; Abcam, ab203035; 1/200), anti-CD4 ((Rat; Biolegend, 100412; 1/200), anti-K14 (Chicken, Thermo Fisher Scientific, #MA5-11599, 1:2000), anti-activeYap1 (Rabbit; Abcam, ab205270; 1/200), anti-Phospho-Myosin Light Chain 2 (Rabbit; Cell signalling, 3674S; 1/200), Phalloidin (Invitrogen, A22287; 1/400), EdU (ThermoFisher, c10340), anti-CC3 (Rabbit; R&D, AF835 ; 1/400), anti-Lamin5 (Rabbit; Abcam, ab14509 ; 1/200). The following secondary antibodies were used (dilution 1:400): anti-rabbit, anti-rat, anti-chicken and anti-goat conjugated either to Alexa Fluor 488 (Molecular Probes) or Rhodamine Red-X (Jackson ImmunoResearch) or Cyanine5 (Jackson ImmunoResearch).

For RNA-Scope, the following mouse probes were used: Mm-Col1a1 (319371) and MmCol1a2 (585461-C2).

For immunochemistry, the following primary antibodies were used : Col1 (Abcam ab270993, 1/1000).

For epidermal whole mount, the following primary antibodies were used: anti-Integrinβ4 (rat, 1:200, BD Biosciences, 346-11A), Keratin 14 (Chicken, Thermo Fisher Scientific, #MA5-11599, 1:2000), Keratin 10 (rabbit; Covance, 905404 ; 1:1000), anti-BrdU (rat, 1:200, Abcam), anti-CC3 (Rabbit; R&D, AF835, 1:600), anti-activeYap1 (Rabbit; Abcam, ab205270; 1/200) and Phalloidin (Invitrogen, A22287; 1/200). The following secondary antibodies were used (dilution 1:400 except for Cyanine5 1/1000): anti-rabbit, anti-rat, anti-chicken and anti-goat conjugated either to Alexa Fluor 488 (Molecular Probes) or Rhodamine Red-X (Jackson ImmunoResearch) or Cyanine5 (Jackson ImmunoResearch).

Validation

The other antibodies used are commercially available and were validated by the provider. We used protocols and recommandations of the manufacturer on validated species. We used positive and negative control tissues to validate the specificity of the stainings.

Animals and other research organisms

Policy information about studies involving animals; ARRIVE guidelines recommended for reporting animal research, and Sex and Gender in Research

Laboratory animals

The K14CreER transgenic mouse model was generated and provided by E. Fuchs laboratory, Rockefeller University, USA. This mouse model is available at the Jackson Laboratory, stock # 005107. The Rosa26-LSL-SMOM2-YFP mouse line was imported from the Jackson Laboratory (stock # 005130). The Rosa26-LSL-mT/mG mouse line was imported from the Jackson Laboratory (stock # 07576). The iChr2-Control-Mosaic was provided by Rui Benedito's lab and is now available in Jackson Laboratory (stock # 031302). All mice used in this study were composed of males and females with mixed genetic backgrounds. Mice were induced between 1.5 and 4 months of age (apart from the experiment on old mice in which the mice were 18 months old) with tamoxifen (Sigma-Aldrich) dissolved in 10% Ethanol and 90% sunflower oil (Sigma). The quantity of tamoxifen administrated to mice was adapted in accordance with their weight. For non-clonal induction: mice were treated with a single intraperitoneal injection (IP) of tamoxifen at a dosage of 1mg/30g. For clonal induction : mice were treated with a single intraperitoneal injection of tamoxifen at a dosage of 0,075mg/30g (ear skin clonal dose) or 0,4mg/30g (back skin clonal dose). Mice were sacrificed at different time points post induction. The housing conditions of all animals were strictly following the ethical regulations. The room temperature ranged from 20 and 24°C. The relative ambient humidity at the level of mouse cages was 55±10%. Each cage was provided with food, water and two types of nesting material. A semi-natural light cycle of 12:12 was used. All the experiments complied strictly with the protocols approved by ethical committee.

Wild animals

No wild animals were used in this study.

Reporting on sex

All mice used in this study were composed of males and females with mixed genetic backgrounds.

Field-collected samples

No field collected sample were used in this study.

Ethics oversight

All animals procedures were approved by the corresponding ethical committee (Commission d'Ethique et du Bien Être Animal (CEBEA), Faculty of Medicine, Université Libre de Bruxelles) under protocol numbers 794 and 820. CEBEA follows the European Convention for the Protection of Vertebrate Animals used for Experimental and other Scientific Purposes. This study is therefore compliant with all ethical regulations regarding animal researches.

Note that full information on the approval of the study protocol must also be provided in the manuscript.

Flow Cytometry

Plots

Confirm that:

☒ The axis labels state the marker and fluorochrome used (e.g. CD4-FITC).

☒ The axis scales are clearly visible. Include numbers along axes only for bottom left plot of group (a 'group' is an analysis of identical markers).

☒ All plots are contour plots with outliers or pseudocolor plots.

☒ A numerical value for number of cells or percentage (with statistics) is provided.

Methodology

Sample preparation

To isolate skin epidermal cells, ears were dissected, opened in two along the cartilage with forceps and incubated in DMEM (Dubelcco's Modified Eagle's Medium- Gibco, thermo Fisher Scientific) - 0,25% Trypsin (Gibco, Thermo Fisher Scientific) overnight at 4°C. The back skin was first shaved with electric clippers, dissected and the hypodermis was then removed by scratching it with a scalpel. The remaining tissue (epidermis-dermis) was finally incubated in DMEM-0,25% trypsin overnight at 4°C by placing the dermis in contact with the solution. The day after, the epidermis was carefully separated from the dermis by using a scalpel and then incubated on a rocking plate (100 rpm) at room temperature for 5 min. Trypsin was neutralized by adding DMEM supplemented with 5% of Chelex-treated Fetal Calf Serum (CFCS) and epidermal cells were mechanically dissociated by pipetting 10 times. Samples were filtrated on a 70µm filter then on a 40µm filter and washed in a PBS-2% CFCS. Single cells were incubated with a biotinylated anti-CD34 primary antibody (clone RAM34; BD Biosciences; dilution 1:50) diluted in PBS-2% CFSC, for one hour on ice on a rocking plate, and protected from light. Cells were washed with PBS-2% CFCS, incubated for 45 min on ice, on a rocking plate, with streptavidin-APC secondary antibody (BD Biosciences; 1:400), washed again and finally resuspended in a Hoechst (10mg/ml) solution diluted at 1:4000 in PBS-2% CFCS.

Instrument	Cell sorting was performed on a BD FACS Aria II at the ULB Flow Cytometry
Software	We used FACSDiva software.
Cell population abundance	SmoM2 mutated cells were isolated based on the expression of the YFP fused to the oncogene. Smom2-YFP expressing cells from the hair follicle bulge were excluded by the CD34-APC staining. For wild type tissues living IFE and infundibulum cells were sorted on the negative expression of the CD34 marker only. 20 000 cells were sorted for each sample and the samples harvested from three different mice were pooled together to obtain a total number of 60 000 cells for both tissues: ear skin and back skin.
Gating strategy	Living epidermal cells were gated by forward scatter, side scatter, and negative for Hoechst

☒ Tick this box to confirm that a figure exemplifying the gating strategy is provided in the Supplementary Information.